Aus der Klinik für Radiologie
der Medizinischen Fakultät Charité – Universitätsmedizin Berlin

DISSERTATION

Quantitative bildbasierte Prädiktoren der Yttrium-90 Verteilung und des Tumoransprechens nach transarterieller Radioembolisation maligner Lebertumoren

Quantitative Imaging Biomarkers for Yttrium-90 Distribution and Tumor Response after Transarterial Radioembolization in malignant Liver Tumors

zur Erlangung des akademischen Grades
Medical Doctor - Doctor of Philosophy (MD/PhD)

vorgelegt der Medizinischen Fakultät
Charité – Universitätsmedizin Berlin

von

Isabel Theresa Schobert

aus Herrenberg

Datum der Promotion: 05.03.2021

Contents

I Abstract

Deutsch

This research was originally published in JNM. Schobert I, Chapiro J, Nezami N, Hamm CA, Gebauer B, Lin M, Pollak J, Saperstein L, Schlachter T, Savic LJ. Quantitative Imaging Biomarkers for (90)Y Distribution on Bremsstrahlung SPECT After Resin-Based Radioembolization. J Nucl Med. 2019;60(8):1066-72. © SNMMI

Dieser Abstract wurde von der obenstehenden Publikation adaptiert und übersetzt.

Zielsetzung: Die Identifizierung prätherapeutischer bildbasierter Tumorcharakteristika zur Vorhersage der Yttrium-90 (^{90}Y) Verteilung in der posttherapeutischen Bremsstrahlung single photon emission computed tomography (SPECT) und des Tumoransprechens in Patienten mit primären und sekundären Lebertumoren nach selektiver interner Radiotherapie (SIRT).

Methoden: In diese retrospektive Studie wurden 38 Patienten mit Lebertumoren, die mit Harzmikrosphären-basierter SIRT behandelt wurden, eingeschlossen. Die Patientenkohorte bestand aus 23 Patienten mit Hepatozellulärem Karzinom (HCC) und 15 Patienten mit anderen malignen Lebertumoren (non-HCC). Die Bildgebung umfasste eine multiphasische Kontrastmittel-MRT oder CT vor SIRT und eine Bremsstrahlung SPECT unmittelbar nach SIRT. Das totale und kontrastmittelaufnehmende Tumorvolumen (ETV [cm^3] and %), und die totale und kontrastmittelaufnehmende Tumorlast (%) wurden volumetrisch auf der prätherapeutischen Bildgebung quantifiziert. Bis zu zwei dominante Tumore pro behandeltem Leberlappen wurden analysiert. Nach der multimodalen Bildregistrierung von prätherapeutischer MRT oder CT auf die SPECT/CT, wurde die ^{90}Y Verteilung in der SPECT als Tumor-zu-normale-Leber Verhältnis (TNR) volumetrisch bestimmt. Das Tumoransprechen wurde anhand der quantitative European Association for the Study of the Liver (qEASL) und response evaluation criteria in solid tumors 1.1 (RECIST1.1) Kriterien beurteilt. Klinische Parameter, wie z.B. Child-Pugh Stadien, wurden ebenfalls untersucht. Statistische Tests umfassten den nicht-parametrischen Mann-Whitney U, die bivariate Pearson Korrelation und Lineare Regression.

Ergebnisse: In HCC korrelierte ein höheres prätherapeutisches ETV% mit höherer TNR in der SPECT, und damit mehr ^{90}Y Aufnahme des Tumors relativ zum umliegenden Lebergewebe ($P<0.001$). In non-HCC bestand die Korrelation zwischen höherer ETV%

und TNR auch (P=0.039). Zusätzlich zeigten HCC Patienten mit Child-Pugh B signifikant mehr ^{90}Y Ablagerung in nicht-tumoröser Leber, gemessen als niedrigere TNR, als Child-Pugh A Patienten (P=0.021). Die Nachsorge-Bildgebung für die Beurteilung des Tumoransprechens innerhalb von 4 Monaten nach SIRT war nach 25 Behandlungen vorhanden. Eine höhere TNR korrelierte mit besserem Tumoransprechen, gemessen als posttherapeutische Reduktion von ETV%, in HCC (P=0.039), aber nicht in non-HCC (P=0.886).

Schlussfolgerung: Diese Studie identifizierte ETV% als quantifizierbaren prätherapeutischen bildbasierten Biomarker für die ^{90}Y Verteilung in der posttherapeutischen Bremsstrahlung SPECT in Patienten mit HCC und non-HCC. Zusätzlich war bei Patienten mit HCC, jedoch nicht bei Patienten mit non-HCC, eine höhere relative ^{90}Y Aufnahme des Tumors mit besserem Tumoransprechen nach SIRT assoziiert.

English

This research was originally published in JNM. Schobert I, Chapiro J, Nezami N, Hamm CA, Gebauer B, Lin M, Pollak J, Saperstein L, Schlachter T, Savic LJ. Quantitative Imaging Biomarkers for (90)Y Distribution on Bremsstrahlung SPECT After Resin-Based Radioembolization. J Nucl Med. 2019;60(8):1066-72. © SNMMI
This abstract was adapted from the above-mentioned publication.

Purpose: To investigate baseline tumor imaging features that predict Yttrium-90 (^{90}Y) distribution on posttreatment single photon emission computed tomography (SPECT) and tumor response to ^{90}Y-transarterial radioembolization (TARE) in patients with primary and secondary liver tumors.

Methods: This retrospective study included 38 patients with liver tumors who underwent resin-based TARE. The patient cohort consisted of 23 patients with hepatocellular carcinoma (HCC) and 15 patients with non-HCC hepatic malignancies. Multiphasic contrast-enhanced magnetic resonance imaging (MRI) or computed tomography (CT) scans were obtained prior to TARE, and Bremsstrahlung SPECT scans were captured immediately post-radioembolization. Total and enhancing tumor volume (ETV [cm^3] and %), and total and enhancing tumor burden (%) were quantified on baseline MRI or CT. Up to two dominant tumors per treated liver lobe were included in the analysis. Non-rigid multimodal image registration of baseline scans and SPECT/CT was performed, and ^{90}Y distribution was volumetrically assessed on posttreatment SPECT as tumor-to-normal-liver ratio (TNR). Tumor response was assessed according to established quantitative European Association for the Study of the Liver criteria (qEASL) and RECIST1.1 criteria. Clinical parameters, such as Child-Pugh class, were also assessed. Statistical analyses included non-parametric Mann-Whitney U test, bivariate Pearson correlation, and linear regression.

Results: In HCC, higher ETV% on baseline imaging correlated with increased TNR on posttreatment SPECT, thus demonstrating higher ^{90}Y-microsphere uptake in tumor relative to liver parenchyma ($P<0.001$). In non-HCC, higher baseline ETV% similarly correlated with increased TNR on SPECT ($P=0.039$). Moreover, HCC patients with Child-Pugh B showed more ^{90}Y-microsphere deposition in nontumorous liver parenchyma, measured as lower TNR, compared to Child-Pugh A patients ($P=0.021$). Follow-up imaging within four months, and in turn response assessment, was available after 25

treatments. Higher TNR correlated with better tumor response, measured as a reduction of ETV% after treatment, in HCC (P=0.039), but not in non-HCC (P=0.886).

Conclusion: In patients with HCC and non-HCC, ETV% may serve as a quantifiable baseline imaging biomarker to predict ^{90}Y distribution on posttreatment Bremsstrahlung SPECT. Moreover, relatively higher tumor ^{90}Y uptake was associated with better tumor response in patients with HCC, though this association was not evident in patients with non-HCC.

II. Manteltext

Background

Hepatocellular Carcinoma (HCC) is the third leading cause of cancer-related deaths with increasing incidence rates worldwide (1). Additionally, the liver is the primary site for metastases of various malignancies, such as colorectal cancer and neuroendocrine tumors (2). In clinics, HCC is staged according to Barcelona Clinic Liver Cancer (BCLC), which takes into account tumor parameters, such as tumor size and number, liver function according to Child-Pugh, and Eastern Cooperative Oncology Group (ECOG) performance status (3). Each BCLC class is linked with specific treatment recommendations (3). HCC is usually diagnosed at intermediate to advanced disease stages, where curative treatments are no longer amenable (4). In these patients, palliative intra-arterial liver-directed therapies (IAT) are guideline-approved and thought to prolong overall survival (OS), bridge or downstage the tumor to liver transplant, and improve Quality of Life (QoL) (5).

IATs comprise various techniques that utilize different materials for intra-arterial injection and varying mechanisms of action (6). Yttrium-90 transarterial radioembolization (^{90}Y-TARE) is mainly used for the treatment of BCLC C patients but is also frequently performed in hepatic metastases such as colorectal cancer liver metastases or neuroendocrine liver metastases (5, 6). The pathophysiological principle of IATs is based on the dual blood supply of the liver parenchyma and liver malignancies. While the liver is mainly supplied by the portal vein, liver tumors are predominantly fed by the hepatic artery (7, 8). Moreover, many liver tumors are hypervascularized with a high microvascular density and a dense peritumoral arterial supply (9).

This unique characteristic of liver tumors is also exploited by ^{90}Y-TARE. During the treatment, a catheter is advanced to a branch of the hepatic artery, and microspheres loaded with radioactive ^{90}Y are delivered to the tumor feeding arteries, while sparing most of the surrounding healthy liver tissue from unnecessary internal radiation (10). The microspheres, which are 20-60 µm in diameter, are trapped in the capillary bed of the tumor where the ^{90}Y undergoes β^- decay into inactive ^{90}Zirconium, and thus irradiates the surrounding tissue over the course of several days (11, 12). ^{90}Y has a half-life of 64.1 hours (11). Due to their diameter, the ^{90}Y-microspheres predominantly accumulate in the tumoral microvasculature, as they cannot pass the capillary bed (13).

There are two types of commercially available ^{90}Y-loaded microspheres that are approved for the treatment of liver malignancies: resin-based microspheres (SIR-Spheres®, Sirtex medical limited, New South Wales, Australia) and glass-based microspheres (TheraSphere®, BTG, London, UK) (11). As compared to glass-based spheres, resin-based microspheres are larger in diameter and have less activity per microsphere (11). Therefore, a higher number of microspheres is injected to achieve comparable doses (11). However, despite those differences between available microspheres, clinical results are comparable (14).

Prior to radioembolization, the individual anatomy of the patient is assessed with a planning angiography combined with a Technetium-99m macroaggregated albumin (^{99m}Tc-MAA) single photon emission computed tomography (SPECT) imaging (12). This is done in order to assess hepatic and extrahepatic vasculature, identify tumor-feeding vessels, and measure shunting to the lungs and gastroenteric organs (12). For resin-based radioembolization, a lung shunt fraction (LSF) of more than 20% is usually a contraindication for treatment. Additionally, the absorbed dose of the lung is calculated prior to therapy using the LSF and the total administered dose. If the estimated absorbed lung dose is <30 Gy, a potential radiation damage such as radiation pneumonitis is unlikely and TARE can be performed (12). Even though the ^{99m}Tc-MAA scan is mandatory and useful in clinical practice to anticipate ^{90}Y-microsphere distribution, the prognostic value is limited due to differences in distribution behavior of the particles (15). The difference in ^{99m}Tc-MAA and ^{90}Y-microsphere uptake may be due to slightly different particle sizes, 10-50 µm for ^{99m}Tc-MAA and 20-60 µm for ^{90}Y resin-microspheres, aggregation of albumin particles, catheter tip positions, which can be different due to separate sessions of the planning scan and the treatment, specific gravity, and the number of infused particles (15, 16). Thus, the ^{99m}Tc-MAA scan helps the nuclear medicine physician plan the intended radiation doses, but does not simulate the ^{90}Y TARE completely (15).

For resin-based TARE, the planned ^{90}Y activity for each patient is calculated with the body surface are (BSA) method, which was developed to achieve safe activities (12). However, it does neither take into account varying ^{90}Y-microsphere distribution nor a personalized tumor absorbed dose target. This results in safe, but sometimes not sufficient injected activities and absorbed doses (17).

In order to assess ^{90}Y deposits after TARE, a ^{90}Y Bremsstrahlung SPECT immediately after TARE is used to visualize the ^{90}Y-microspheres and evaluate the

coverage of the tumor, non-target deposits to healthy liver parenchyma, and shunting to neighboring organs (12). In recent investigations, the quantitative assessment of ^{90}Y activity distribution and calculation of absorbed doses based on SPECT have proven technically advanced but feasible (18). However, the application of quantitative SPECT for the prediction of outcome after radioembolization remains challenging due to varying ^{90}Y-microspheres uptake and dose-response relationships of individual tumors across entities and within the same entity (17, 19).

The activity distribution and deposits of ^{90}Y-microspheres can also be assessed with positron emission tomography (PET), because of the internal pair production of ^{90}Y (20). Even though the use of PET may be easier to quantify absorbed doses due to an incorporated calibration algorithm and higher spatial resolution, SPECT is due to cost-efficiency more widely available and was thus used in this study as well (21).

It has been shown that sufficient coverage of the tumor with ^{90}Y leads to reliable tumor response (19). For resin-based radioembolization it is recommended to administer a mean tumor absorbed dose of at least 120 Gy, in order to achieve tumor response and to limit liver absorbed doses to less than 50 Gy, and lung absorbed doses to less than 20 Gy to prevent radiation-related toxicity (22). As ^{90}Y-microspheres usually do not distribute evenly in the tumor, studies analyzing dose-volume-histograms on PET/CT after ^{90}Y resin-microsphere TARE showed that at least 70% of the tumor volume needs to be covered with at least 100 Gy, in order to result in complete response in patients with HCC (19).

As the effect of TARE relies on radiation-induced DNA damage, tumor response, if measured as tumor size reduction, occurs as late as two to six months after treatment (23). Compared to other IATs, this interval is rather long (e.g. only four weeks after TACE) causing a delayed response assessment and thus, a suboptimal setting for non-responders requiring additional treatments. This is particularly problematic for palliative patients and makes an early estimate of treatment success and probability of tumor response very much needed.

The biology and vasculature of hepatic metastases such as colorectal cancer liver metastases differ from HCC. This leads to a deviation in general appearance on imaging and contrast agent uptake behavior compared to HCC (24, 25). For example, colorectal cancer liver metastases show hypointense signal on T1 weighted images and an enhancing rim after contrast administration, but usually the necrotic center of the metastasis remains hypovascular (24). Because particle distribution after TARE follows

arterial perfusion, in large colorectal liver metastases often only few particles are distributed into the necrotic hypovascular center (11). Studies investigating tumor response parameters in colorectal liver metastases that predict overall survival after TARE found volumetric measurements of tumor metabolism, such as total lesion glycolysis and metabolic tumor volume quantified on FDG-PET, to be an early surrogate marker for the outcome after TARE (26). Additionally, CT perfusion imaging early after treatment was found to correlate with tumor response after ^{90}Y-TARE (27).

Most primary liver cancer develop in cirrhotic livers, that do not only show decreased liver function but also major changes in liver structure and matrix composition (3). Those alterations in parenchymal structure lead for example to portal hypertension, hepatofugal portal blood flow, hepatic artery buffer response, and intrahepatic shunting of blood (28, 29). The above-mentioned changes in hemodynamics are relevant to intra-arterial therapies, which rely on liver vasculature and tumor capillary beds (12).

Given the heterogenous ^{90}Y microsphere distribution within the liver and the importance of early response prediction in palliative patients, this study aimed on the one hand to identify imaging surrogate markers for ^{90}Y distribution on Bremsstrahlung SPECT, and on the other hand investigate the effect of ^{90}Y distribution on tumor response after TARE.

Methodology

This research was originally published in JNM. *Schobert I, Chapiro J, Nezami N, Hamm CA, Gebauer B, Lin M, Pollak J, Saperstein L, Schlachter T, Savic LJ. Quantitative Imaging Biomarkers for (90)Y Distribution on Bremsstrahlung SPECT After Resin-Based Radioembolization. J Nucl Med. 2019;60(8):1066-72. © SNMMI*
The following text describes the already published Material and Methods in detail.

Study Cohort

This retrospective study is compliant with the Health Insurance Portability and Accountability Act of 1996 (HIPAA) and was approved by the institutional review board (IRB) of Yale University. Due to the retrospective design of the study, informed consent was waived. The study cohort comprises 38 patients, 23 with HCC and 15 with other hepatic malignancies. Patients were included if they had primary or secondary liver malignancies, treated with lobar and resin-based TARE, treatment date between August

2012 and January 2018, and received contrast-enhanced imaging within three months prior to treatment and a SPECT/CT immediately after treatment. Exclusion criteria were tumor size smaller than 1.5 cm, no SPECT imaging immediately after TARE, insufficient image quality of the CT, MRI or SPECT, and segmental treatment. A minimum tumor size was important due to the partial volume effect and spatial resolution (30). Some patients dropped out as they received only a planar scan after treatment, due to reimbursement system regulations. And image quality had to allow for (quantitative) image analysis. In total, 38 patients with 40 treated lobes and 58 dominant tumors were included in the analysis. Additionally, clinical parameters such as Child-Pugh class were assessed.

MRI and CT Imaging

Prior to treatment all patients received contrast-enhanced CT or MR imaging of the abdomen (baseline imaging) and after 25 radioembolizations, patients received follow-up imaging within one to four months. Imaging was performed according to standardized institutional protocols. Briefly, patients received non-contrast and contrast-enhanced multi-phasic T1-weighted scans on a 1.5T MRI (Magnetom Avanto; Siemens; Erlangen, Germany) using a phased-array torso coil. The standardized protocol included T1-weighted breath-hold non-contrast and contrast enhanced imaging in the hepatic arterial phase (20 seconds after contrast administration), portalvenous (70 seconds after contrast administration), and venous phase (3 minutes after contrast administration). For contrast-enhanced imaging 0.1 mmol/kg intravenous macrocyclic gadolinium-based contrast agent (Dotarem; Guerbet, Roissy, France) was used. The multi-phasic contrast-enhanced CT was acquired with a multi-detector scanner (Siemens, Malvern, USA, PA) and included native scans, contrast-enhanced arterial, portal-venous, and venous phases.

^{90}Y Radioembolization

The preparation of TARE included an angiography of the mesentery and tumor supplying arteries and a ^{99m}Tc-MAA scan one or two weeks prior to treatment in order to assess the lung shunt fraction and reduce the planned dose of ^{90}Y if needed. Dose calculation was performed using the BSA model.

For the ^{90}Y-TARE, the hepatic artery was catheterized under fluoroscopy guidance via transfemoral access. Then, a microcatheter was advanced through the catheter and placed either in the proximal left or the right hepatic artery for digital subtraction

angiography (DSA) and lobar injection of ^{90}Y resin-microspheres (SIR-Spheres; SIRTeX Medical Limited; Lane Cove, Australia). In case of bilobar treatment, the lobar administrations of ^{90}Y were performed sequentially with at time interval of three to four weeks.

SPECT/CT

Immediately after completion of TARE, a Bremsstrahlung SPECT/CT was acquired. The dual-head SPECT scanner (Symbia Truepoint; Siemens; Malvern, PA) had a Low-Energy High-Resolution collimator. Besides planar scans, SPECT images were acquired. Images were acquired with 32 frames per camera and 20 seconds per frame. The acquisition energy windows were 55-100 keV and 105-195 keV and matrix size was 128x128. The CT was acquired low-dose with 130kV, 0.8 seconds rotation time, 30mAs, and a matrix size of 512x512. Data was reconstructed with the iterative ordered subset expectation maximization (OSEM) method using FLASH 3D, a company-specific software. The SPECT was then visualized with and without fusion to the CT.

3D Tumor Image Analysis

Up to two tumors per treated lobe were defined as dominant tumors, depending on the largest diameter. The tumor boundaries and liver lobe boundaries were volumetrically outlined (segmented) on the T1-weighted MRI or CT in arterial contrast phase. The segmentation and measurement of the total tumor volume (TTV in cm3) and total liver lobe volume was done on baseline and follow-up imaging using semi-automatic interactive 3D software (GeoBlend Software). For the quantification of tumor enhancement, a software called quantitative European Association for the Study of the Liver (qEASL, Intellispace Portal, Philips Healthcare; Best, Netherlands) was used. Besides measuring the absolute enhancing tumor volume (ETV in cm3), the relative enhancing tumor volume (ETV%) was calculated as the ratio of ETV and TTV. The qEASL software workflow included the following: the non-contrast images were subtracted from the arterial phase images to remove background signal. The volumetrically segmented tumor mask was then applied to the subtracted image and a reference box was placed in surrounding non-tumorous liver parenchyma. The definition of tumor contrast enhancement was every voxel that had at least two standard deviations higher signal intensity compared to the reference box in the liver parenchyma, as previously described (31). Thus, tumor enhancement was defined voxel-by-voxel based on an individual

threshold. Moreover, the volumetrically outlined liver lobes were used to calculate the total and enhancing tumor burden of the lobes to be treated with TARE. The above described parameters will hereinafter be called imaging biomarkers for ^{90}Y-microsphere distribution. Regarding tumor response assessment, the change of ETV% and tumor diameter after treatment were calculated and categorized according to previously described qEASL% and RECIST 1.1 criteria as complete response, partial response, stable disease, and progressive disease.

^{90}Y Biodistribution

The ^{90}Y-SPECT scans were loaded into MIM Encore (MIM Software Inc.; Cleveland, OH), a nuclear medicine software, and analyzed with a dedicated image analysis protocol. Treated liver lobes and the dominant tumors were volumetrically outlined on the baseline arterial phase images. SPECT images were reconstructed with an algorithm that included scatter and attenuation correction. The baseline arterial phase MRI or CT was non-rigidly registered to the CT of the hybrid ^{90}Y-SPECT/CT and was afterwards fused to the SPECT. In order to achieve a healthy liver lobe parenchyma volume without tumorous volume, all non-dominant tumors were also volumetrically segmented and subtracted from the healthy liver lobe. Thereafter, the total number of counts was quantified in the dominant tumors and in the non-tumorous treated liver lobe. The activity per count was determined as follows: the LSF was subtracted from the total injected activity and the remaining activity was divided by the total number of counts within the liver. Eventually, to measure the distribution of ^{90}Y to the tumorous and non-tumorous tissue within the treated liver lobe, the tumor-to-normal-liver-ratio (TNR) was calculated as a ratio of counts within the dominant tumors and healthy liver lobe parenchyma.

For the conversion of the SPECT-based count rate into a measure of activity concentration, phantom experiments were conducted, in order to calculate a calibration correction factor (CCF) as previously described. Thereafter, absorbed dose calculations were done according to the partition model.

Statistical Analysis

Descriptive data, for the characterization of the patient cohort and tumors at baseline, was summarized as absolute (n) and relative (%) frequency, mean and standard deviation (SD), and median and range. Further correlation and comparative analyses included Pearson correlation test and linear regression analysis for the relationship

between ETV and TNR, and TNR and tumor response. Mann-Whitney-U test was used for the investigation of the impact of liver cirrhosis on ^{90}Y distribution, and Kaplan-Meier analysis was used for median overall survival and survival curves. Statistical analysis was carried out using SPSS (IBM Corp., v24.0, Armonk, New York, USA) and Graphpad Prism (v7.0, La Jolla, California, USA). A two-tailed P-value <0.05 was considered statistically significant.

Essential new results

This research was originally published in JNM. *Schobert I, Chapiro J, Nezami N, Hamm CA, Gebauer B, Lin M, Pollak J, Saperstein L, Schlachter T, Savic LJ. Quantitative Imaging Biomarkers for (90)Y Distribution on Bremsstrahlung SPECT After Resin-Based Radioembolization. J Nucl Med. 2019;60(8):1066-72. © SNMMI*
The following text describes the published results in detail.

Table 1. Baseline patient characteristics. This research was originally published in JNM. Schobert I, Chapiro J, Nezami N, Hamm CA, Gebauer B, Lin M, Pollak J, Saperstein L, Schlachter T, Savic LJ. Quantitative Imaging Biomarkers for (90)Y Distribution on Bremsstrahlung SPECT After Resin-Based Radioembolization. J Nucl Med. 2019;60(8):1066-72. © SNMMI
This table was adapted from the above mentioned publication.

	n (%) HCC	*n* (%) Non-HCC
Number of patients	23 (100)	15 (100)
Male / female	18 (78.26) /5 (21.74)	9 (60) / 6 (40)
Age (years), mean ± SD	62.39 ± 8.62	61.13 ± 11.51
Caucasian / Asian / African-American	18 (78.26) / 1 (4.35) / 4 (17.39)	12 (80) / 1 (6.67) / 2 (13.33)
Cirrhosis	23 (100)	0 (0)
Child-Pugh A / B	13 (56.52) / 10 (43.48)	N/A
ECOG 0 / 1	11 (47.83) / 12 (52.17)	9 (60) / 6 (40)
BCLC B / C	10 (43.45) / 13 (56.52)	N/A

	n (%) HCC	*n* (%) Non-HCC
Pretreatment: Systemic therapies / Resection / Locoregional treatment*	5 (21.74) / 3 (13.04) / 21 (91.3)	10 (66.67) / 3 (20) / 3 (20)

*only non-pretreated tumors were included in analyses

Study Population and Overall Survival

The baseline characteristics of the present cohort are displayed in table 1. The HCC cohort is in the left column, the non-HCC cohort in the right column. The 15 patients with non-HCC had intrahepatic cholangiocarcinoma, and metastases from neuroendocrine cancer, colorectal cancer, melanoma cancer, Prostate cancer, and Leiomyosarcoma. The median overall survival of patients with HCC was 14.4 months (1.58-55.76), and for patients with non-HCC 18.97 months (1.48-55.07). At the end of follow-up, five (21.74%) patients with HCC and ten (66.66%) patients with non-HCC were alive and therefore censored in Kaplan-Meier survival analysis.

Imaging Findings

Patients with HCC had a median of 6 (IQR 3.5–12, range 1–54) tumors in the liver, 4 (2–5, 1–11) tumors per treated liver lobe, and a median tumor burden of 13.05% per treated liver lobe (IQR 5.12–28.78, range 0.71–67.56). Patients with non-HCC malignancies had a median of 11 (IQR 5.5–11, range 4–129) tumors in the liver, 6 (IQR 3.5–6, range 1–85) tumors per treated liver lobe, and a median tumor burden of 6.1% (IQR 5.59–26.73, range 1.53–76.86) per treated liver lobe. The dominant tumors had a mean diameter of 5.24 ± 2.93 cm in the HCC cohort and 4.68 ± 2.48 cm ($p = 0.445$) in the non-HCC cohort, respectively.

Response Assessment

Follow-up imaging for response assessment was available after n=25 treatments. HCC patients had a median time to follow-up imaging of 68 days (range 30-111) and non-HCC patients had a median time to follow-up imaging of 78 days (range 28-143). According to volumetric enhancement-based qEASL%, there was no complete response after TARE, 0 and 2 (28.57%) patients had partial response, 17 (94.44%) and 5 (71.43%) patients had stable disease, and 1 (5.56%) and no patient had progressive disease, in

the HCC and non-HCC cohort, respectively. qEASL% response assessment was used for correlation with TNR. According to unidimensional RECIST1.1, no patient had complete response, 2 (11.11%) patients and 3 (42.86%) patients showed partial response, 15 (83.33%) patients and 4 (57.14%) patients had stable disease, and 1 (5.56%) and no patient had progressive disease, in the HCC and non-HCC cohort, respectively.

^{90}Y and ^{99m}Tc-MAA Distribution and Absorbed Doses

On pre-treatment ^{99m}Tc-MAA SPECT/CT, patients had a mean LSF of 6.6 ± 4.7%. During ^{90}Y-TARE, patients received a mean ^{90}Y activity of 1.17 ± 0.61 GBq and showed a calculated mean absorbed tumor and liver parenchyma dose of 52.52 ± 31.8 and 39.94 ± 22.4 Gy, respectively. The dominant tumors had a mean ^{90}Y distribution ratio, measured as TNR, of 1.47 ± 0.42 in HCC patients and 1.52 ± 0.65 in non-HCC patients.

Correlation of Baseline Tumor Characteristics on Imaging with ^{90}Y-microsphere Distribution on SPECT and Overall Survival

The relationship between ETV% on baseline MRI and ^{90}Y distribution, quantified as TNR on SPECT, was assessed. The two-tailed Pearson correlation demonstrated that HCC with a higher contrast enhancing tumor percentage distributed more ^{90}Y to the tumors ($p < 0.001$). The linear regression model showed a correlation coefficient (r) of 0.759 and a R^2 of 0.516. In non-HCC patients, the correlation of ETV% and TNR was statistically significant ($p = 0.039$), but not as strong as in HCC patients ($r = 0.424$; $R^2 = 0.179$). Moreover, a baseline ETV% threshold value of 80% achieved the most pronounced separation of TNR in patients with HCC ($p < 0.001$) and non-HCC malignancies ($p = 0.014$). Thus, patients with baseline ETV ≥80% distributed on average more ^{90}Y to the tumors than patients with <80% baseline ETV. Regarding the other baseline tumor features, the tumor diameter ($p = 0.488$ and $p = 0.845$), total ($p = 0.109$ and $p = 0.982$) and enhancing tumor volume ($p = 0.43$ and $p = 0.686$), and total ($p = 0.498$ and $p = 0.125$) and enhancing tumor burden ($p = 0.852$ and $p = 0.768$) did not correlate with TNR. Furthermore, in the present cohort, baseline ETV% did not show a significant correlation with overall survival in patients with HCC ($p = 0.088$) and non-HCC ($p = 0.172$).

Correlation of Baseline Clinical Characteristics with ^{90}Y-microsphere Distribution

Besides baseline imaging features such as ETV, the impact of liver cirrhosis on ^{90}Y distribution was assessed. Therefore, in a subanalysis with HCC patients, TNR was stratified according to Child-Pugh classes. In this cohort, patients with Child-Pugh B distributed significantly less ^{90}Y to the tumor compared to Child-Pugh A patients, as revealed by comparison of TNR values with Mann-Whitney U test ($p = 0.021$). Moreover, Child-Pugh B patients distributed significantly more ^{99m}Tc-MAA to the lungs, measured as higher LSF, compared to Child-Pugh A patients ($p = 0.049$).

Correlation of ^{90}Y-microsphere Distribution with Tumor Response

Eventually, ^{90}Y-microsphere distribution and tumor response according to qEASL% were correlated. In HCC, high TNR values on SPECT correlated with better tumor response on follow-up imaging ($p = 0.038$, $r = -0.465$, $R^2 = 0.216$). However, in non-HCC patients, no correlation between TNR and tumor response was found ($p = 0.886$, $R^2 = 0.002$, $r = 0.044$). Of note, there was no significant relation between TNR and overall survival in patients with HCC ($p = 0.526$) or non-HCC ($p = 0.233$).

Resulting clinical applications and further scientific questions

This study identified ETV% on baseline imaging as a quantifiable surrogate marker for ^{90}Y distribution after TARE using 3D image registration and analysis of SPECT, MRI and CT in patients with liver malignancies. Additionally, the relationship between ^{90}Y uptake to the tumor and response to treatment was confirmed in patients with HCC but could not be proven in hepatic metastatic disease.

In the present study, the baseline tumor parameter ETV% was investigated as an easily applicable and non-invasive imaging biomarker and surrogate for ^{90}Y-microsphere distribution to the tumor after TARE ($p < 0.001$). The identification of such non-invasive biomarkers may help improve and refine clinical patient selection for ^{90}Y-TARE and may ultimately help strengthen the role of TARE among other IATs by identifying patients that are most susceptible to TARE and thus most likely to respond. Recently, the effect of TARE was questioned, due to the results of large cohort prospective studies. The multicenter prospective phase III studies SIRveNIB and SARAH compared the outcome after TARE with the standard of care sorafenib in patients with advanced stage HCC (32, 33). Those studies did not find a survival benefit for patients treated with TARE, however, side effects after treatment were lower and quality of life was improved compared to

sorafenib treatment (32, 33). Additionally, SIRveNIB found longer time to progression and progression-free survival after TARE (32). However, patient selection was done based on clinical evaluation of the patients, such as BCLC stage, rather than on individual tumor characteristics. BCLC stage B or C comprise a heterogeneous patient population with varying tumor characteristics, disease extent, and prognosis (3). This rather immature process of patient selection is reflected in clinical decision making as well. If patients are not eligible or have not responded to TACE, TARE is considered. However, institutions which adopted TARE as a primary locoregional therapy for HCC achieved improved overall survival compared to TACE (5). This underscores the need for personalized patient selection and treatment decisions for optimized treatment efficacy.

In theory and as confirmed in this study, hypervascularized tumors with large ETV% at baseline are more likely to take up ^{90}Y microspheres which remain in the capillary bed where they actively irradiate the tumor. In case of unfavorable tumor vascularization and subsequent low contrast uptake, an approach to artificially increase arterial perfusion exists that may increase ^{90}Y-microsphere distribution towards the tumor and thus improve treatment efficacy of TARE (34). Furthermore, advances in microcatheter technology have led to the development of new administration techniques that aim at increased, tumor-targeted delivery of high radiation doses (35). Among these techniques, radiation segmentectomy has evolved which requires placement of the catheter in close proximity to the tumor in a (sub-)segmental artery and thus, increases the ^{90}Y activity to an ablative dose (36). Radiation segmentectomy proved feasible for patients with singular tumors limited to few segments (36). Another new approach to intensify radiation doses is the boosted selective internal radiation therapy (B-SIRT), which aims for a personalized dose prescription, and thus higher doses for patients with a low risk profile for treatment complications (37). In patients with HCC, the ^{99m}Tc-MAA scan was assessed regarding particle distribution to the tumor and healthy liver, and regarding the total injected dose, in order to personalize the ^{90}Y dose. The treatment intensifications with higher tumor absorbed doses achieved better response rates without higher rates of adverse events or toxicity (37). Even though B-SIRT approach was introduced using glass-microspheres in HCC, which generally achieve higher doses more easily, the personalized dosimetry and treatment planning are desirable for resin-based TARE as well. In future research, baseline imaging biomarkers for ^{90}Y distribution and treatment efficacy could be investigated with a radiomics or deep learning approach, in order to find and refine criteria indicative of the individual tumor susceptibility to treatment.

As a second step, based on the preparatory angiography and ^{99m}Tc-MAA scan, a B-SIRT inspired treatment planning would optimize patient selection and therapeutic outcome in clinical practice.

As tumor response generally occurs after a relatively large interval compared to other IATs, early surrogate markers for tumor response prediction are urgently needed to distinguish between responders and non-responders who require additional treatments. Additional challenges in imaging-based tumor response assessment include the frequently observed occurrence of radiation-related edema, which may lead to an increase in tumor size after TARE of varying duration (23). Overall, these example stress the disadvantages of unidimensional, size-based response assessments such as RECIST (23). In turn, they emphasize the importance of enhancement-based measurements in the context of tumor response to IATs. However, early after radioembolization, some tumors show hemorrhage and are thus hyperintense on T1-weighted MRI. Another early finding on post-procedural imaging is treatment-related inflammation within the tumor and in the peritumoral area, which appears as arterial hyperenhancement. Moreover, tumors can display a thin enhancing rim that is related to fibrosis rather than viable tumor (23). Those imaging findings make early response assessment and assessment solely based on the contrast-enhanced images obsolete, as the differentiation between treatment-related changes to the tumor and tumor response remains unclear. These potential pitfalls in image analysis after TARE highlight the potential advantages of qEASL response assessment, which was used in the present study. qEASL uses subtracted images, removing T1 hyperintense signal from arterial phase MRI, thus taking the actual tumor enhancement and the change of enhancement over time into account (38). The study further demonstrates the use of TNR on SPECT as a readily applicable surrogate marker for enhancement-based volumetric tumor response according to qEASL in patients with HCC ($p = 0.038$). As measurable changes in tumor size develop rather late after treatment, TNR may help to assess treatment efficacy early and facilitate clinical treatment planning for palliative patients with little time.

Similar to HCC, non-HCC malignancies also demonstrated that a high enhancing tumor percentage on baseline imaging correlates with ^{90}Y distribution to the tumor on SPECT ($p = 0.039$). However, ^{90}Y distribution was not predictive of tumor response after TARE in these tumors ($p = 0.886$). A possible explanation for this observation could be that the non-HCC cohort comprised several tumor entities. This causes a substantial heterogeneity and may hamper clear results regarding the relationship of TNR with tumor

response. In future works, this may be addressed by investigating each tumor entity separately. Additionally, more recently introduced concepts, such as metabolic tumor response assessment and CT perfusion imaging proved to be valuable for early response prediction in hepatic metastases after TARE (26, 27). Furthermore, diffusion weighted imaging and the quantitative apparent diffusion coefficient proved to be an early predictor for tumor response and survival after radioembolization (39).

Besides tumor type, this study revealed additional predictors of ^{90}Y distribution that take into account the anatomic and structural variability among patients. As the majority of HCC develop in chronic liver disease, liver cirrhosis is a frequently encountered feature and can be found in varying severity, which is assessed by Child-Pugh class (3). The present study showed that patients with impaired liver function and Child-Pugh class B had lower TNR values and higher LSF compared to Child-Pugh A patients. This unfavorable ^{90}Y distribution pattern with relatively more ^{90}Y deposition in the healthy liver parenchyma and lungs may be associated with a higher risk of treatment-related adverse events and toxicity (40). Therefore, advanced cirrhosis may hinder effective and safe treatment and thus, should be considered in pre-treatment patient evaluation in order to select the best possible treatment for each individual patient.

In conclusion, this study showed the value of ETV% as an easily clinically applicable and quantitative imaging surrogate marker on baseline contrast-enhanced imaging for the prediction of ^{90}Y microsphere distribution on SPECT immediately after TARE in primary and secondary hepatic malignancies. Yet, the effect of a favorable ^{90}Y distribution to the tumor on improved treatment response was only shown for HCC. In summary, those imaging biomarkers may help refine patient selection and thus improve outcome after TARE.

References

1. Bray F, Ferlay J, Soerjomataram I, Siegel RL, Torre LA, Jemal A. Global cancer statistics 2018: GLOBOCAN estimates of incidence and mortality worldwide for 36 cancers in 185 countries. CA: a cancer journal for clinicians. 2018;68(6):394-424.
2. Lozano R, Naghavi M, Foreman K, Lim S, Shibuya K, Aboyans V, Abraham J, Adair T, Aggarwal R, Ahn SY, AlMazroa MA, Alvarado M, Anderson HR, Anderson LM, Andrews KG, Atkinson C, Baddour LM, Barker-Collo S, Bartels DH, Bell ML, Benjamin EJ, Bennett D, Bhalla K, Bikbov B, Abdulhak AB, Birbeck G, Blyth F, Bolliger I, Boufous S, Bucello C, Burch M, Burney P, Carapetis J, Chen H, Chou D, Chugh SS, Coffeng LE, Colan SD, Colquhoun S, Colson KE, Condon J, Connor MD, Cooper LT, Corriere M, Cortinovis M, de Vaccaro KC, Couser W, Cowie BC, Criqui MH, Cross M, Dabhadkar KC, Dahodwala N, De Leo D, Degenhardt L, Delossantos A, Denenberg J, Des Jarlais DC, Dharmaratne SD, Dorsey ER, Driscoll T, Duber H, Ebel B, Erwin PJ, Espindola P, Ezzati M, Feigin V, Flaxman AD, Forouzanfar MH, Fowkes FGR, Franklin R, Fransen M, Freeman MK, Gabriel SE, Gakidou E, Gaspari F, Gillum RF, Gonzalez-Medina D, Halasa YA, Haring D, Harrison JE, Havmoeller R, Hay RJ, Hoen B, Hotez PJ, Hoy D, Jacobsen KH, James SL, Jasrasaria R, Jayaraman S, Johns N, Karthikeyan G, Kassebaum N, Keren A, Khoo J-P, Knowlton LM, Kobusingye O, Koranteng A, Krishnamurthi R, Lipnick M, Lipshultz SE, Ohno SL, Mabweijano J, MacIntyre MF, Mallinger L, March L, Marks GB, Marks R, Matsumori A, Matzopoulos R, Mayosi BM, McAnulty JH, McDermott MM, McGrath J, Memish ZA, Mensah GA, Merriman TR, Michaud C, Miller M, Miller TR, Mock C, Mocumbi AO, Mokdad AA, Moran A, Mulholland K, Nair MN, Naldi L, Narayan KMV, Nasseri K, Norman P, O'Donnell M, Omer SB, Ortblad K, Osborne R, Ozgediz D, Pahari B, Pandian JD, Rivero AP, Padilla RP, Perez-Ruiz F, Perico N, Phillips D, Pierce K, Pope CA, Porrini E, Pourmalek F, Raju M, Ranganathan D, Rehm JT, Rein DB, Remuzzi G, Rivara FP, Roberts T, De León FR, Rosenfeld LC, Rushton L, Sacco RL, Salomon JA, Sampson U, Sanman E, Schwebel DC, Segui-Gomez M, Shepard DS, Singh D, Singleton J, Sliwa K, Smith E, Steer A, Taylor JA, Thomas B, Tleyjeh IM, Towbin JA, Truelsen T, Undurraga EA, Venketasubramanian N, Vijayakumar L, Vos T, Wagner GR, Wang M, Wang W, Watt K, Weinstock MA, Weintraub R, Wilkinson JD, Woolf AD, Wulf S, Yeh P-H, Yip P, Zabetian A, Zheng Z-J, Lopez AD, Murray CJL. Global and regional mortality from 235 causes of death for 20 age groups in 1990 and 2010: a systematic analysis for the Global Burden of Disease Study 2010. The Lancet. 2012;380(9859):2095-128.
3. Yang JD, Hainaut P, Gores GJ, Amadou A, Plymoth A, Roberts LR. A global view of hepatocellular carcinoma: trends, risk, prevention and management. Nature reviews Gastroenterology & hepatology. 2019;16(10):589-604.
4. Park JW, Chen M, Colombo M, Roberts LR, Schwartz M, Chen PJ, Kudo M, Johnson P, Wagner S, Orsini LS, Sherman M. Global patterns of hepatocellular carcinoma management from diagnosis to death: the BRIDGE Study. Liver international : official journal of the International Association for the Study of the Liver. 2015;35(9):2155-66.
5. Salem R, Gabr A, Riaz A, Mora R, Ali R, Abecassis M, Hickey R, Kulik L, Ganger D, Flamm S, Atassi R, Atassi B, Sato K, Benson AB, Mulcahy MF, Abouchaleh N, Asadi AA, Desai K, Thornburg B, Vouche M, Habib A, Caicedo J, Miller FH, Yaghmai V, Kallini JR, Mouli S, Lewandowski RJ. Institutional decision to adopt Y90 as primary treatment for hepatocellular carcinoma informed by a 1,000-patient 15-year experience. Hepatology. 2018;68(4):1429-40.
6. Talenfeld AD, Sista AK, Madoff DC. Transarterial Therapies for Primary Liver Tumors. Surgical Oncology Clinics. 2014;23(2):323-51.
7. Breedis C, Young G. The blood supply of neoplasms in the liver. The American journal of pathology. 1954;30(5):969-77.
8. Lewandowski RJ, Salem R. Yttrium-90 radioembolization of hepatocellular carcinoma and metastatic disease to the liver. Seminars in interventional radiology. 2006;23(1):64-72.
9. Choi BI, Han JK, Cho JM, Choi DS, Han MC, Lee HS, Kim CY. Characterization of focal hepatic tumors. Value of two-phase scanning with spiral computed tomography. Cancer. 1995;76(12):2434-42.

10. Lewandowski RJ, Salem R. Yttrium-90 radioembolization of hepatocellular carcinoma and metastatic disease to the liver. Seminars in interventional radiology. 2006;23(1):64-72.
11. Westcott MA, Coldwell DM, Liu DM, Zikria JF. The development, commercialization, and clinical context of yttrium-90 radiolabeled resin and glass microspheres. Advances in Radiation Oncology. 2016;1(4):351-64.
12. Kallini JR, Gabr A, Salem R, Lewandowski RJ. Transarterial Radioembolization with Yttrium-90 for the Treatment of Hepatocellular Carcinoma. Adv Ther. 2016;33(5):699-714.
13. Venkatanarasimha N, Gogna A, Tong KTA, Damodharan K, Chow PKH, Lo RHG, Chandramohan S. Radioembolisation of hepatocellular carcinoma: a primer. Clin Radiol. 2017;72(12):1002-13.
14. Van Der Gucht A, Jreige M, Denys A, Blanc-Durand P, Boubaker A, Pomoni A, Mitsakis P, Silva-Monteiro M, Gnesin S, Lalonde MN, Duran R, Prior JO, Schaefer N. Resin Versus Glass Microspheres for (90)Y Transarterial Radioembolization: Comparing Survival in Unresectable Hepatocellular Carcinoma Using Pretreatment Partition Model Dosimetry. J Nucl Med. 2017;58(8):1334-40.
15. Ilhan H, Goritschan A, Paprottka P, Jakobs TF, Fendler WP, Todica A, Bartenstein P, Hacker M, Haug AR. Predictive Value of 99mTc-MAA SPECT for 90Y-Labeled Resin Microsphere Distribution in Radioembolization of Primary and Secondary Hepatic Tumors. J Nucl Med. 2015;56(11):1654-60.
16. Van de Wiele C, Maes A, Brugman E, D'Asseler Y, De Spiegeleer B, Mees G, Stellamans K. SIRT of liver metastases: physiological and pathophysiological considerations. European Journal of Nuclear Medicine and Molecular Imaging. 2012;39(10):1646-55.
17. van den Hoven AF, Rosenbaum CE, Elias SG, de Jong HW, Koopman M, Verkooijen HM, Alavi A, van den Bosch MA, Lam MG. Insights into the Dose-Response Relationship of Radioembolization with Resin 90Y-Microspheres: A Prospective Cohort Study in Patients with Colorectal Cancer Liver Metastases. J Nucl Med. 2016;57(7):1014-9.
18. Kappadath SC, Mikell J, Balagopal A, Baladandayuthapani V, Kaseb A, Mahvash A. Hepatocellular Carcinoma Tumor Dose Response After (90)Y-radioembolization With Glass Microspheres Using (90)Y-SPECT/CT-Based Voxel Dosimetry. Int J Radiat Oncol Biol Phys. 2018;102(2):451-61.
19. Kao Y-H, Steinberg JD, Tay Y-S, Lim GKY, Yan J, Townsend DW, Budgeon CA, Boucek JA, Francis RJ, Cheo TST, Burgmans MC, Irani FG, Lo RHG, Tay K-H, Tan B-S, Chow PKH, Satchithanantham S, Tan AEH, Ng DCE, Goh ASW. Post-radioembolization yttrium-90 PET/CT - part 2: dose-response and tumor predictive dosimetry for resin microspheres. EJNMMI Research. 2013;3(1):57.
20. Elschot M, Vermolen BJ, Lam MG, de Keizer B, van den Bosch MA, de Jong HW. Quantitative comparison of PET and Bremsstrahlung SPECT for imaging the in vivo yttrium-90 microsphere distribution after liver radioembolization. PLoS One. 2013;8(2):e55742.
21. Hicks RJ, Hofman MS. Is there still a role for SPECT–CT in oncology in the PET–CT era? Nature Reviews Clinical Oncology. 2012;9:712.
22. Lau W-Y, Kennedy AS, Kim YH, Lai HK, Lee R-C, Leung TWT, Liu C-S, Salem R, Sangro B, Shuter B, Wang S-C. Patient Selection and Activity Planning Guide for Selective Internal Radiotherapy With Yttrium-90 Resin Microspheres. International Journal of Radiation Oncology*Biology*Physics. 2012;82(1):401-7.
23. Joo I, Kim H-C, Kim GM, Paeng JC. Imaging Evaluation Following (90)Y Radioembolization of Liver Tumors: What Radiologists Should Know. Korean Journal of Radiology. 2018;19(2):209-22.
24. Sica GT, Ji H, Ros PR. CT and MR imaging of hepatic metastases. AJR Am J Roentgenol. 2000;174(3):691-8.
25. Shah S, Shukla A, Paunipagar B. Radiological Features of Hepatocellular Carcinoma. Journal of Clinical and Experimental Hepatology. 2014;4:S63-S6.
26. Shady W, Kishore S, Gavane S, Do RK, Osborne JR, Ulaner GA, Gonen M, Ziv E, Boas FE, Sofocleous CT. Metabolic tumor volume and total lesion glycolysis on FDG-PET/CT can predict overall survival after (90)Y radioembolization of colorectal liver metastases: A

comparison with SUVmax, SUVpeak, and RECIST 1.0. European journal of radiology. 2016;85(6):1224-31.
27. Reiner CS, Morsbach F, Sah BR, Puippe G, Schaefer N, Pfammatter T, Alkadhi H. Early treatment response evaluation after yttrium-90 radioembolization of liver malignancy with CT perfusion. J Vasc Interv Radiol. 2014;25(5):747-59.
28. Vignaux O, Gouya H, Augui J, Oudjit A, Coste J, Dousset B, Chaussade S, Legmann P. Hepatofugal portal flow in advanced liver cirrhosis with spontaneous portosystemic shunts: effects on parenchymal hepatic enhancement at dual-phase helical CT. Abdominal imaging. 2002;27(5):536-40.
29. Molino G, Bar F, Battista S, Torchio M, Niro AG, Garello E, Avagnina P, Fava C, Grosso M, Spalluto F. Arterial-venous shunting in liver cirrhosis. Digestive diseases and sciences. 1998;43(1):51-5.
30. Shady W, Sotirchos VS, Do RK, Pandit-Taskar N, Carrasquillo JA, Gonen M, Sofocleous CT. Surrogate Imaging Biomarkers of Response of Colorectal Liver Metastases After Salvage Radioembolization Using 90Y-Loaded Resin Microspheres. AJR Am J Roentgenol. 2016;207(3):661-70.
31. Chockalingam A, Duran R, Sohn JH, Schernthaner R, Chapiro J, Lee H, Sahu S, Nguyen S, Geschwind JF, Lin M. Radiologic-pathologic analysis of quantitative 3D tumour enhancement on contrast-enhanced MR imaging: a study of ROI placement. European radiology. 2016;26(1):103-13.
32. Chow PKH, Gandhi M, Tan SB, Khin MW, Khasbazar A, Ong J, Choo SP, Cheow PC, Chotipanich C, Lim K, Lesmana LA, Manuaba TW, Yoong BK, Raj A, Law CS, Cua IHY, Lobo RR, Teh CSC, Kim YH, Jong YW, Han HS, Bae SH, Yoon HK, Lee RC, Hung CF, Peng CY, Liang PC, Bartlett A, Kok KYY, Thng CH, Low AS, Goh ASW, Tay KH, Lo RHG, Goh BKP, Ng DCE, Lekurwale G, Liew WM, Gebski V, Mak KSW, Soo KC. SIRveNIB: Selective Internal Radiation Therapy Versus Sorafenib in Asia-Pacific Patients With Hepatocellular Carcinoma. Journal of clinical oncology : official journal of the American Society of Clinical Oncology. 2018;36(19):1913-21.
33. Vilgrain V, Pereira H, Assenat E, Guiu B, Ilonca AD, Pageaux GP, Sibert A, Bouattour M, Lebtahi R, Allaham W, Barraud H, Laurent V, Mathias E, Bronowicki JP, Tasu JP, Perdrisot R, Silvain C, Gerolami R, Mundler O, Seitz JF, Vidal V, Aube C, Oberti F, Couturier O, Brenot-Rossi I, Raoul JL, Sarran A, Costentin C, Itti E, Luciani A, Adam R, Lewin M, Samuel D, Ronot M, Dinut A, Castera L, Chatellier G. Efficacy and safety of selective internal radiotherapy with yttrium-90 resin microspheres compared with sorafenib in locally advanced and inoperable hepatocellular carcinoma (SARAH): an open-label randomised controlled phase 3 trial. The Lancet Oncology. 2017;18(12):1624-36.
34. Sasaki Y, Imaoka S, Hasegawa Y, Nakano S, Ishikawa O, Ohigashi H, Taniguchi K, Koyama H, Iwanaga T, Terasawa T. Changes in distribution of hepatic blood flow induced by intra-arterial infusion of angiotensin II in human hepatic cancer. Cancer. 1985;55(2):311-6.
35. Riaz A, Gates VL, Atassi B, Lewandowski RJ, Mulcahy MF, Ryu RK, Sato KT, Baker T, Kulik L, Gupta R, Abecassis M, Benson AB, 3rd, Omary R, Millender L, Kennedy A, Salem R. Radiation segmentectomy: a novel approach to increase safety and efficacy of radioembolization. Int J Radiat Oncol Biol Phys. 2011;79(1):163-71.
36. Lewandowski RJ, Gabr A, Abouchaleh N, Ali R, Al Asadi A, Mora RA, Kulik L, Ganger D, Desai K, Thornburg B, Mouli S, Hickey R, Caicedo JC, Abecassis M, Riaz A, Salem R. Radiation Segmentectomy: Potential Curative Therapy for Early Hepatocellular Carcinoma. Radiology. 2018;287(3):1050-8.
37. Garin E, Lenoir L, Edeline J, Laffont S, Mesbah H, Poree P, Sulpice L, Boudjema K, Mesbah M, Guillygomarc'h A, Quehen E, Pracht M, Raoul JL, Clement B, Rolland Y, Boucher E. Boosted selective internal radiation therapy with 90Y-loaded glass microspheres (B-SIRT) for hepatocellular carcinoma patients: a new personalized promising concept. Eur J Nucl Med Mol Imaging. 2013;40(7):1057-68.
38. Tacher V, Lin M, Duran R, Yarmohammadi H, Lee H, Chapiro J, Chao M, Wang Z, Frangakis C, Sohn JH, Maltenfort MG, Pawlik T, Geschwind JF. Comparison of Existing

Response Criteria in Patients with Hepatocellular Carcinoma Treated with Transarterial Chemoembolization Using a 3D Quantitative Approach. Radiology. 2016;278(1):275-84.
39. Alis D, Durmaz ESM, Gulsen F, Bas A, Kabasakal L, Sager S, Numan F. Prognostic value of ADC measurements in predicting overall survival in patients undergoing (90)Y radioembolization for colorectal cancer liver metastases. Clin Imaging. 2019;57:124-30.
40. Gabrielson A, Miller A, Banovac F, Kim A, He AR, Unger K. Outcomes and Predictors of Toxicity after Selective Internal Radiation Therapy Using Yttrium-90 Resin Microspheres for Unresectable Hepatocellular Carcinoma. Front Oncol. 2015;5:292.

III. Affidavit / Eidesstattliche Versicherung

„Ich, Isabel Theresa Schobert, versichere an Eides statt durch meine eigenhändige Unterschrift, dass ich die vorgelegte Dissertation mit dem Thema: *Quantitative bildbasierte Prädiktoren der Yttrium-90 Verteilung und des Tumoransprechens nach transarterieller Radioembolisation maligner Lebertumoren / Quantitative Imaging Biomarkers for Yttrium-90 Distribution and Tumor Response after Transarterial Radioembolization in malignant Liver Tumors* selbstständig und ohne nicht offengelegte Hilfe Dritter verfasst und keine anderen als die angegebenen Quellen und Hilfsmittel genutzt habe.
Alle Stellen, die wörtlich oder dem Sinne nach auf Publikationen oder Vorträgen anderer Autoren/innen beruhen, sind als solche in korrekter Zitierung kenntlich gemacht. Die Abschnitte zu Methodik (insbesondere praktische Arbeiten, Laborbestimmungen, statistische Aufarbeitung) und Resultaten (insbesondere Abbildungen, Graphiken und Tabellen) werden von mir verantwortet.

Ich versichere ferner, dass ich die in Zusammenarbeit mit anderen Personen generierten Daten, Datenauswertungen und Schlussfolgerungen korrekt gekennzeichnet und meinen eigenen Beitrag sowie die Beiträge anderer Personen korrekt kenntlich gemacht habe (siehe Anteilserklärung). Texte oder Textteile, die gemeinsam mit anderen erstellt oder verwendet wurden, habe ich korrekt kenntlich gemacht.

Meine Anteile an etwaigen Publikationen zu dieser Dissertation entsprechen denen, die in der untenstehenden gemeinsamen Erklärung mit dem Erstbetreuer, angegeben sind. Für sämtliche im Rahmen der Dissertation entstandenen Publikationen wurden die Richtlinien des ICMJE (International Committee of Medical Journal Editors; www.icmje.og) zur Autorenschaft eingehalten. Ich erkläre ferner, dass ich mich zur Einhaltung der Satzung der Charité – Universitätsmedizin Berlin zur Sicherung Guter Wissenschaftlicher Praxis verpflichte.

Weiterhin versichere ich, dass ich diese Dissertation weder in gleicher noch in ähnlicher Form bereits an einer anderen Fakultät eingereicht habe.

Die Bedeutung dieser eidesstattlichen Versicherung und die strafrechtlichen Folgen einer unwahren eidesstattlichen Versicherung (§§156, 161 des Strafgesetzbuches) sind mir bekannt und bewusst.“

Datum Unterschrift

IV. Detailed statement of contributions / Ausführliche Anteilserklärung an der erfolgten Publikation als Top-Journal im Rahmen der Promotionsverfahren zum MD/PhD

Publikation 1: Schobert I, Chapiro J, Nezami N, Hamm CA, Gebauer B, Lin M, Pollak J, Saperstein L, Schlachter T, Savic LJ. Quantitative Imaging Biomarkers for (90)Y Distribution on Bremsstrahlung SPECT After Resin-Based Radioembolization. J Nucl Med. 2019;60(8):1066-72.

Beitrag im Einzelnen:
- Literaturrecherche
- Konzept und Design der Studie gemeinsam mit den Betreuern
- Patientenselektion und Charakterisierung der Studienkohorte, Sammlung der Daten
- Definition der Einschluss- und Ausschlusskriterien
- Durchsicht und Interpretation der klinischen Patientenberichte und der Bildgebung
- Software-basierte Bildanalyse der MRT und CT mit Segmentierung der Tumore und Leberlappen in der Baseline- und Nachsorgebildgebung
- Software-basierte (qEASL) Berechnung des enhancing tumor volume (ETV), der Tumorlast und der kontrastmittelaufnehmenden Tumorlast
- Beurteilung des Tumoransprechens anhand der qEASL und RECIST 1.1 Kriterien
- Software-basierte multimodale Bildanalyse der SPECT: Konzipierung eines Bildanalyseprotokolls in der MIM Encore software, Segmentierung der Tumore und Leberlappen in der MRT oder CT, nicht-rigide Bildregistrierung der baseline Bildgebung auf die CT der SPECT/CT und dann auf die SPECT. Bestimmung der counts innerhalb der Segmentierungen, Berechnung der Aktivität pro count und tumor-to-normal-liver-ratio (TNR). Konzipierung der Phantomstudie, Mithilfe bei der Durchführung der Phantomstudie (Phantomvorbereitung, Supervision), Berechnung des calibration correction factors (CCF) und der absorbierten Strahlendosis der Patienten
- Wahl und Durchführung der Statistik mit Überprüfung durch Statistiker
- Wahl und Durchführung der Datenvisualisierung (Tabellen und Graphen)
- Entwurf des Manuskripts inklusive Literaturwahl, Revision anhand der Anmerkungen der Betreuer, Einreichung bei JNM und Adressierung der Kommentare der Reviewer
- Vorstellung der Studie auf wissenschaftlichen Kongressen

_____
Unterschrift, Datum und Stempel des/der erstbetreuenden Hochschullehrers/in

_____
Unterschrift des Doktoranden/der Doktorandin

V. Excerpt of journal summary list

Journal Data Filtered By: **Selected JCR Year: 2017** Selected Editions: SCIE,SSCI
Selected Categories: **"RADIOLOGY, NUCLEAR MEDICINE and MEDICAL IMAGING"** Selected Category Scheme: WoS
Gesamtanzahl: 128 Journale

Rank	Full Journal Title	Total Cites	Journal Impact Factor	Eigenfactor Score
1	JACC-Cardiovascular Imaging	8,104	10.247	0.026360
2	European Heart Journal-Cardiovascular Imaging	4,630	8.336	0.020640
3	EUROPEAN JOURNAL OF NUCLEAR MEDICINE AND MOLECULAR IMAGING	14,983	7.704	0.024870
4	RADIOLOGY	54,109	7.469	0.063710
5	JOURNAL OF NUCLEAR MEDICINE	27,101	7.439	0.037560
6	CLINICAL NUCLEAR MEDICINE	4,756	6.281	0.006950
7	INVESTIGATIVE RADIOLOGY	6,486	6.224	0.012410
8	Circulation-Cardiovascular Imaging	5,438	6.221	0.020160
9	IEEE TRANSACTIONS ON MEDICAL IMAGING	17,837	6.131	0.024200
10	ULTRASOUND IN OBSTETRICS & GYNECOLOGY	12,420	5.654	0.018820
11	INTERNATIONAL JOURNAL OF RADIATION ONCOLOGY BIOLOGY PHYSICS	46,595	5.554	0.055060
12	JOURNAL OF CARDIOVASCULAR MAGNETIC RESONANCE	4,918	5.457	0.013530
13	NEUROIMAGE	92,719	5.426	0.152610
14	MEDICAL IMAGE ANALYSIS	6,383	5.356	0.011900
15	RADIOTHERAPY AND ONCOLOGY	17,184	4.942	0.027840
16	HUMAN BRAIN MAPPING	20,334	4.927	0.042810
17	SEMINARS IN NUCLEAR MEDICINE	2,285	4.558	0.002990
18	ULTRASCHALL IN DER MEDIZIN	2,201	4.389	0.004310
19	MAGNETIC RESONANCE IN MEDICINE	31,440	4.082	0.034130
20	EUROPEAN RADIOLOGY	18,615	4.027	0.034120
20	SEMINARS IN RADIATION ONCOLOGY	2,480	4.027	0.003620
22	JOURNAL OF NUCLEAR CARDIOLOGY	3,508	3.847	0.004120
23	AMERICAN JOURNAL OF NEURORADIOLOGY	22,667	3.653	0.029840
24	JOURNAL OF MAGNETIC RESONANCE IMAGING	16,398	3.612	0.027440
25	MOLECULAR IMAGING AND BIOLOGY	2,415	3.608	0.005480

Quantitative Imaging Biomarkers for ^{90}Y Distribution on Bremsstrahlung SPECT After Resin-Based Radioembolization

Isabel Schobert[1,2], Julius Chapiro[1], Nariman Nezami[1], Charlie A. Hamm[1,2], Bernhard Gebauer[2], MingDe Lin[1,3], Jeffrey Pollak[1], Lawrence Saperstein[1], Todd Schlachter[1], and Lynn J. Savic[1,2]

[1]Department of Radiology and Biomedical Imaging, Yale School of Medicine, New Haven, Connecticut; [2]Institute of Radiology, Charité Universitätsmedizin Berlin, Corporate Member of Freie Universität Berlin, Humboldt-Universität, and Berlin Institute of Health, Berlin, Germany; and [3]Visage Imaging Inc., San Diego, California

Our purpose was to identify baseline imaging features in patients with liver cancer that correlate with ^{90}Y distribution on postprocedural SPECT and predict tumor response to transarterial radioembolization (TARE). **Methods:** This retrospective study was approved by the institutional review board and included 38 patients with hepatocellular carcinoma (HCC) (n = 23; 18/23 men; mean age, 62.39 ± 8.62 y; 34 dominant tumors) and non-HCC hepatic malignancies (n = 15; 9/15 men; mean age, 61.13 ± 11.51 y; 24 dominant tumors) who underwent 40 resin-based TARE treatments (August 2012 to January 2018). Multiphasic contrast-enhanced MRI or CT was obtained before and Bremsstrahlung SPECT within 2 h after TARE. Total tumor volume (cm^3) and enhancing tumor volume (ETV [cm^3] and % of total tumor volume), and total and enhancing tumor burden (%), were volumetrically assessed on baseline imaging. Up to 2 dominant tumors per treated lobe were analyzed. After multimodal image registration of baseline imaging and SPECT/CT, ^{90}Y distribution was quantified on SPECT as tumor–to–normal-liver ratio (TNR). Response was assessed according to RECIST1.1 and quantitative European Association for the Study of the Liver criteria. Clinical parameters were also assessed. Statistical tests included Mann–Whitney *U,* Pearson correlation, and linear regression. **Results:** In HCC patients, high baseline ETV% significantly correlated with high TNR on SPECT, demonstrating greater ^{90}Y uptake in the tumor relative to the liver parenchyma ($P < 0.001$). In non-HCC patients, a correlation between ETV% and TNR was observed as well (P = 0.039). Follow-up imaging for response assessments within 1–4 mo after TARE was available for 23 patients with 25 treatments. The change of ETV% significantly correlated with TNR in HCC (P = 0.039) but not in non-HCC patients (P = 0.886). Additionally, Child–Pugh class B patients demonstrated significantly more ^{90}Y deposition in nontumorous liver than Child–Pugh A patients (P = 0.021). **Conclusion:** This study identified ETV% as a quantifiable imaging biomarker on preprocedural MRI and CT to predict ^{90}Y distribution on postprocedural SPECT in HCC and non-HCC. However, the relationship between the preferential uptake of ^{90}Y to the tumor and tumor response after radioembolization could be validated only for HCC.

Key Words: radioembolization; ^{90}Y; quantitative SPECT; contrast enhancement; imaging biomarker

J Nucl Med 2019; 60:1066–1072
DOI: 10.2967/jnumed.118.219691

Hepatocellular carcinoma (HCC) is the sixth most common cancer and the third most common cause of cancer-related deaths worldwide (*1*). Moreover, liver is the primary metastatic site for many malignancies, especially of gastrointestinal origin such as colorectal carcinoma or neuroendocrine tumors (*2*). Over 70% of newly diagnosed patients with primary or secondary liver cancer present with advanced disease stages and are no longer amenable for curative therapeutic approaches (*3,4*). In this setting, intraarterial therapies such as transarterial chemoembolization (TACE) and radioembolization (TARE) with ^{90}Y constitute mainstay palliative treatment options (*5*).

In TARE, microspheres loaded with radioactive ^{90}Y are injected into the hepatic artery to deliver therapeutic doses of radiation to the liver lobe that contains the target tumors. The particles are trapped and remain in the tumor capillary bed, where they decay with β^--emissions (*6*). Radiation is the predominant therapeutic effect of TARE, whereas the embolic properties of the 20- to 60-μm microspheres remain limited and depend on the total number of administered microspheres. In fact, angiographic stasis before complete dose delivery occurs in only about 20% of treatments (*7,8*).

Previous studies have shown that ^{90}Y uptake of the target tumors corresponds with tumor response to treatment (*9*). A clinically used tool to predict ^{90}Y biodistribution before TARE is the preparatory ^{99m}Tc-macroaggregated albumin (^{99m}Tc-MAA) scan. However, the prognostic value of ^{99m}Tc-MAA for ^{90}Y deposition patterns is limited mainly by different particle sizes and hemodynamics, which restricts the relevance of the ^{99m}Tc-MAA scan to the identification of hepatopulmonary shunting (*10*).

For post-TARE evaluation of ^{90}Y distribution in clinical practice, deposits are visualized on Bremsstrahlung SPECT immediately after treatment to qualitatively assess ^{90}Y distribution to the tumor and liver tissue as well as nontarget deposition and shunting to other organs. More recently, quantitative methods for SPECT analysis have been investigated for the measurement of ^{90}Y distribution and calculation of absorbed doses and proved technically feasible in an experimental setting (*11*). However, as ^{90}Y uptake of tumors and dose–response relationships are highly variable across

Received Sep. 5, 2018; revision accepted Dec. 19, 2018.
For correspondence or reprints contact: Julius Chapiro, Department of Radiology and Biomedical Imaging, Yale School of Medicine, 300 Cedar St., TAC N312A, New Haven, CT 06520.
E-mail: julius.chapiro@yale.edu
Published online Jan. 17, 2019.

tumors of different etiology and morphology, the use of quantitative ^{90}Y-SPECT for the prediction of tumor response to TARE remains challenging.

Therefore, this study aimed to identify and establish baseline imaging features in patients with liver malignancies that predict ^{90}Y distribution as seen on post-TARE Bremsstrahlung SPECT and to assess the prognostic value of ^{90}Y distribution for early prediction of tumor response.

MATERIALS AND METHODS

Study Cohort

This Health Insurance Portability and Accountability Act–compliant, retrospective single-center study was approved by the institutional review board, and informed consent was waived. In total, 38 patients with 23 HCC and 15 non-HCC liver malignancies who received lobar resin-based ^{90}Y-TARE between August 2012 and January 2018 were included. The relatively high dropout rate due to missing SPECT was related to reimbursement system regulations that stipulated planar scans instead of SPECT. Forty treated liver lobes with 58 dominant tumors were included in the final analysis. With respect to partial-volume effect and limited spatial resolution of SPECT imaging, tumors smaller than 1.5 cm in diameter were excluded from the analysis (Fig. 1) (*12*). Clinical parameters were also assessed.

MRI and CT Imaging

All patients received either MRI or CT of the liver before (baseline) and after 25 treatments 1–4 mo after the TARE procedure (follow-up). Scans were acquired according to the respective standardized institutional protocols. Specifically, patients underwent contrast-enhanced multiphasic T1-weighted MRI with a 1.5-T scanner (Magnetom Avanto; Siemens) using a phased-array torso coil. The protocol included breath-hold unenhanced and contrast-enhanced (intravenous macrocyclic gadolinium) imaging in the hepatic arterial (20 s after administration), portal venous (70 s), and delayed phase (3 min). The multiphasic contrast-enhanced CT was performed with a multidetector scanner (Siemens) including native, arterial, portal venous, and delayed contrast-enhanced phases.

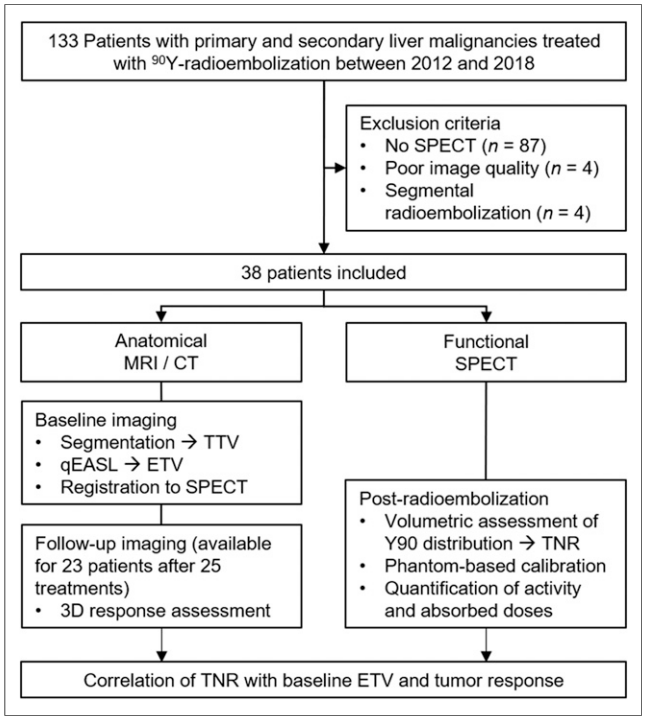

FIGURE 1. Study workflow and exclusion criteria.

TARE

Within 2 wk before TARE, all patients underwent mesenteric angiography to identify the vascular supply of the tumor and a ^{99m}Tc-MAA scan to calculate the lung shunt fraction (LSF) and subsequent dose reduction.

For the actual treatment, a catheter was placed via transfemoral access under fluoroscopy guidance. Thereafter, a microcatheter was advanced into a proximal hepatic artery branch for lobar administration of ^{90}Y resin-microspheres (SIR-Spheres; SIRTeX Medical Limited). For bilobar therapy, the interval between sequential treatments was 3–4 wk.

SPECT/CT

Within 2 h after completion of TARE, Bremsstrahlung SPECT/CT was performed. The dual-head scanner (Symbia TruePoint; Siemens) was equipped with a low-energy high-resolution collimator. Acquisition settings included 32 frames per camera and a 20-s acquisition time per frame. Matrix size was 128 × 128, and energy windows were 55–100 and 105–195 keV. The low-dose CT was acquired with 130 kV, 30 mAs, 0.8-s rotation time, and 512 × 512 matrix. Maximum-likelihood reconstruction based on 3-dimensional (3D) ordered-subsets expectation maximization was performed using a manufacturer-specific software (FLASH 3D).

3D Tumor Assessment on MRI and CT

Up to 2 dominant target tumors per treated lobe were determined by size and segmented in 3 dimensions on the arterial-phase T1-weighted MRI or CT scans at baseline and follow-up using a semiautomated, volumetric technique to measure the total tumor volume (TTV, cm^3). Quantitative European Association for the Study of the Liver (IntelliSpace Portal; Philips Healthcare), a software-based 3D quantification tool, was used to calculate the absolute enhancing tumor volume (ETV, cm^3) and the ETV in percentage of the TTV (ETV%). Briefly, the precontrast scan was subtracted from the arterial-phase scan to remove background enhancement. The 3D segmented tumor mask was applied, and a reference region was placed in healthy liver parenchyma. Tumor enhancement was defined as 2 SDs above the signal intensity of the reference region as previously described (*13*). In addition, the treated liver lobes were segmented, and the total and enhancing tumor burden per treated lobe were assessed (*14*). These parameters are referred to here as imaging biomarkers for ^{90}Y distribution.

For volumetric tumor response assessment, changes of TTV, ETV, and ETV% between baseline and follow-up imaging were calculated and interpreted according to the established qEASL% criteria (*13,14*). Additionally, tumor response was assessed according to RECIST1.1. Response was categorized as complete or partial response or as stable or progressive disease.

^{90}Y Biodistribution

^{90}Y SPECT images were analyzed with a dedicated protocol in MIM Encore (MIM Software Inc.). Treated lobes and dominant tumors were volumetrically segmented on the baseline contrast-enhanced MRI or CT, which was nonrigidly registered to the CT of the SPECT/CT and then to the scatter- and attenuation-corrected SPECT. All remaining tumors in the treated lobe were also segmented, and the volumes were subtracted from the liver lobe volume to separate the healthy liver parenchyma from tumorous tissue. On the basis of these segmentations, the total number of counts in the dominant tumors and the nontumorous parenchyma of the treated lobe were quantified. ^{90}Y activity per count was calculated on the basis of the administered dose, the LSF, and the total number of counts within the

TABLE 1
Baseline HCC Patient Characteristics

Parameter	*n* (%)
Demographics	
Number of patients	23 (100)
Age (y), mean ± SD	62.39 ± 8.62
Male/female	18 (78.26)/5 (21.74)
Ethnicity	
Caucasian	18 (78.26)
Asian	1 (4.35)
African-American	4 (17.39)
Disease characteristics	
Etiology of cirrhosis	
Viral hepatitis	17 (73.91)
Alcohol consumption	4 (17.39)
Nonalcoholic steatohepatitis	2 (8.7)
Eastern Cooperative Oncology Group performance status	
0	11 (47.83)
1	12 (52.17)
Child–Pugh class	
A	13 (56.52)
B	10 (43.48)
Barcelona Clinic liver cancer stage	
B	10 (43.45)
C	13 (56.52)
Main portal vein thrombosis	5 (21.74)
Extrahepatic disease	3 (13.04)
Tumor characteristics, median (interquartile range, range)	
Number of tumors/liver	6 (3.5–12, 1–54)
Number of tumors/analyzed lobe	4 (2–5, 1–11)
TTV (cm^3)/analyzed lobe	110.08 (79.82–225.58, 4.13–730.37)
ETV (cm^3)/analyzed lobe	62.57 (7.47–112.8, 0–509.95)
Tumor burden (%)/analyzed lobe	13.05 (5.12–28.78, 0.71–67.56)
Enhancing tumor burden (%)/analyzed lobe	4.34 (0.83–12.41, 0–57.82)
Previous treatments	
Sorafenib	5 (21.74)
Resection*	3 (13.04)
TACE*	11 (47.83)
Ablation*	5 (21.74)
Other	5 (21.74)

*Pretreated tumors are not included in the analysis.

TABLE 2
Baseline Non-HCC Patient Characteristics

Parameter	*n* (%)
Demographics	
Number of patients	15 (100)
Age (y), mean ± SD	61.13 ± 11.51
Male/female	9 (60)/6 (40)
Ethnicity	
Caucasian	12 (80)
Asian	1 (6.67)
African-American	2 (13.33)
Disease characteristics	
Tumor entity	
Intrahepatic cholangiocarcinoma	2 (13.33)
Neuroendocrine cancer metastases	7 (46.67)
Colorectal cancer metastases	3 (20)
Melanoma cancer metastases	1 (6.67)
Prostate cancer metastases	1 (6.67)
Leiomyosarcoma metastases	1 (6.67)
Eastern Cooperative Oncology Group performance status	
0	9 (60)
1	6 (40)
Main portal vein thrombosis	1 (6.67)
Tumor characteristics, median (interquartile range, range)	
Number of tumors/liver	11 (5.5–11, 4–129)
Number of tumors/analyzed lobe	6 (3.5–6, 1–85)
TTV (cm^3)/analyzed lobe	102.01 (67.03–300.89, 14.94–1,868.39)
ETV (cm^3)/analyzed lobe	66.66 (19.54–87.79, 0–839.01)
Tumor burden/analyzed lobe (%)	6.1 (5.59–26.73, 1.53–76.86)
Enhancing tumor burden/analyzed lobe (%)	4.38 (2.12–5.45, 0–38.25)
Previous treatments	
Systemic therapies	10 (66.67)
Resection*	3 (20)
TACE*	1 (6.67)
Ablation*	2 (13.33)

*Pretreated tumors are not included in the analysis.

liver. Finally, the tumor–to–normal-liver ratio (TNR) was calculated, representing the distribution of ^{90}Y between the dominant tumors and nontumorous liver in the treated lobe.

To convert the count-rate on the SPECT image to a measure of activity concentration, a phantom-based calibration correction factor was calculated of 4 phantom studies as previously described (*11*). Briefly, activity concentrations measured on SPECT were divided by

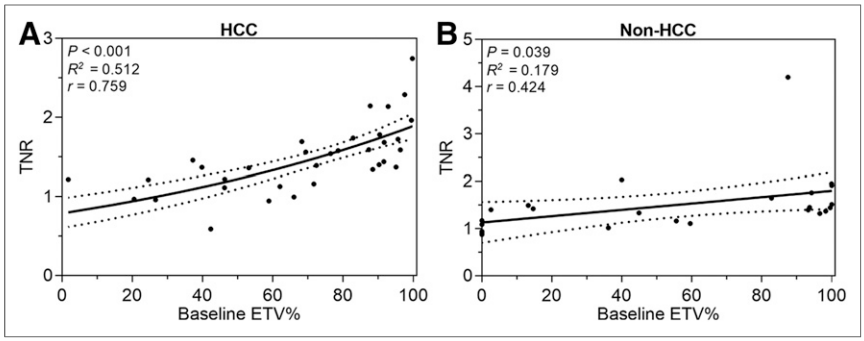

FIGURE 2. Correlation of baseline ETV% and ^{90}Y distribution after TARE. This graph demonstrates that with greater ETV% on baseline imaging, ^{90}Y uptake of tumor measured as TNR increases in HCC ($n = 34$, $P < 0.001$) (A) as well as non-HCC ($n = 24$, $P = 0.039$) (B). Intermittent lines indicate 95% confidence interval.

the true activity concentrations measured at the time of the scan using an activity meter to obtain the calibration correction factor (Supplemental Fig. 1; supplemental materials are available at http://jnm.snmjournals.org). The 4 results were averaged and multiplied by the counts within the volume of interest. Eventually, absorbed doses were calculated using partition modeling (*15*).

Statistical Analysis

Descriptive results are reported as frequency (*n, %*), mean ± SD, or median and range. Further analyses included Pearson correlation, linear regression, Mann–Whitney *U* test, and Kaplan–Meier curves. Statistical analyses were performed using SPSS (IBM Corp., version 24.0) and Prism (version 7.0). A *P* value of less than 0.05 was considered statistically significant.

RESULTS

Study Population and Survival Analysis

Detailed characteristics of the patient population are displayed in Tables 1 and 2. Patients with HCC and non-HCC had a median survival of 14.4 (1.58–55.76) and 18.97 (1.48–55.07) months after TARE, respectively. Five patients with HCC and 10 patients with non-HCC were still alive at the end of follow-up and censored for Kaplan–Meier analysis.

Imaging Findings

Baseline Imaging Features. The tumor characteristics on baseline MRI or CT are displayed in Tables 1 and 2. The dominant tumors measured 5.24 ± 2.93 cm and 4.68 ± 2.48 cm ($P = 0.445$) for HCC and non-HCC, respectively.

Response Assessment. Follow-up imaging was acquired within a median time of 68 (30–111) and 78 (28–143) days for HCC and non-HCC, respectively, and was available after 25 treatments. According to 3D enhancement-based qEASL%, which was further used for correlation analyses with TNR, TARE achieved no complete responses, 0 and 2 (28.57%) partial responses, 17 (94.44%) and 5 (71.43%) stable disease, and 1 (5.56%) and 0 progressive disease in HCC and non-HCC, respectively. According to RECIST1.1, there was no complete response, 2 (11.11%) and 3 (42.86%) partial responses, 15 (83.33%) and 4 (57.14%) stable disease, and 1 (5.56%) and 0 progressive disease in HCC and non-HCC, respectively.

^{90}Y Distribution on SPECT/CT and Absorbed Dose Calculations. Patients had a mean ^{99m}Tc-MAA LSF of 6.6% ± 4.7%. The mean administered activity was 1.17 ± 0.61 GBq, and the mean absorbed tumor and healthy liver dose were 52.52 ± 31.8 and 39.94 ± 22.4 Gy, respectively. The mean ^{90}Y distribution to the dominant tumors quantified as TNR was 1.47 ± 0.42 in HCC and 1.52 ± 0.65 in non-HCC.

Correlation Analyses

Correlation of Baseline Imaging Features with ^{90}Y Distribution and Survival. The 2-tailed Pearson analysis revealed a significant correlation between baseline ETV% and ^{90}Y distribution on SPECT quantified as TNR, showing that more relative enhancement was associated with higher TNR in patients with HCC ($P < 0.001$). The correlation coefficient (r) was 0.759 and R^2 was 0.516 in a linear regression model. In patients with liver cancer other than HCC, the correlation of baseline ETV% with TNR was not as strong as in HCC but still statistically significant ($P = 0.039$; $r = 0.424$; $R^2 = 0.179$) (Fig. 2). Specifically, a baseline ETV% cutoff of 80% was empirically identified to provide the most significant separation of TNR values in HCC ($P < 0.001$) and non-HCC patients ($P = 0.014$), demonstrating higher mean TNR for patients with ETV% of at least 80% (Fig. 3). As for the remaining baseline tumor characteristics, TTV ($P = 0.109$ and 0.982), ETV ($P = 0.43$ and 0.686), diameter ($P = 0.488$ and 0.845), tumor burden ($P = 0.498$ and 0.125), and enhancing tumor burden ($P = 0.852$ and 0.768) did not demonstrate significant correlations with TNR. Of note, survival did not correlate with baseline ETV% in HCC ($P = 0.088$) and non-HCC ($P = 0.172$).

Correlation of Baseline Clinical Features with ^{90}Y Distribution. To assess the effect of liver cirrhosis on the ^{90}Y distribution, Child–Pugh classes were correlated with TNR. In the present cohort, the mean TNR of Child–Pugh B patients was significantly lower than that of Child–Pugh A patients ($P = 0.021$) (Fig. 4). Furthermore, patients with Child–Pugh B had a significantly higher LSF than Child–Pugh A ($P = 0.049$).

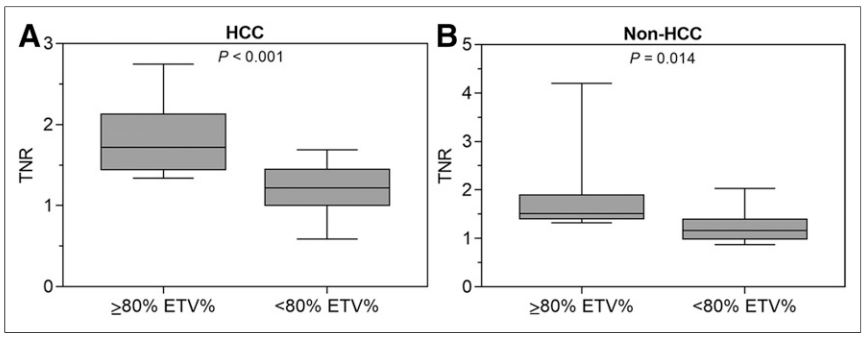

FIGURE 3. Stratification of ^{90}Y distribution according to tumor enhancement thresholds. Mann–Whitney-*U* test reveals 80% baseline ETV% as empirically most significant cutoff value to stratify patients with HCC ($P < 0.001$) (A) and non-HCC ($P = 0.014$) (B) according to TNR. Graph shows median, range, and 25th–75th percentiles.

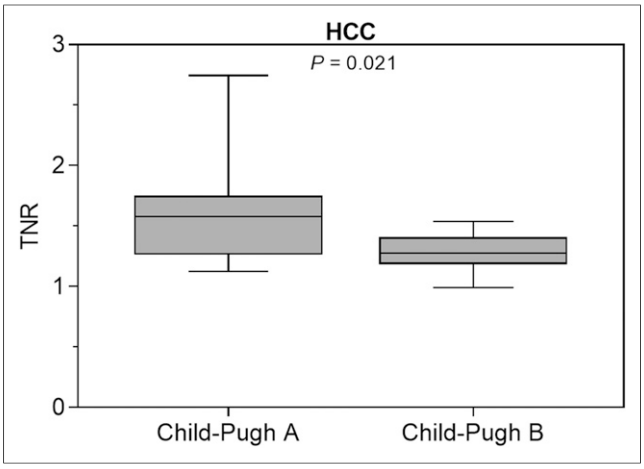

FIGURE 4. Stratification of ^{90}Y distribution according to Child–Pugh class. HCC patients with Child–Pugh B show significantly decreased TNR compared with Child–Pugh A ($P = 0.021$). Graph shows median, range, and 25th–75th percentiles.

Correlation of ^{90}Y Distribution with Tumor Response. Furthermore, ^{90}Y distribution was correlated with tumor response available in a subset of patients ($n = 25$). For HCC, a high TNR correlated with tumor response according to the enhancement-based volumetric qEASL% criteria ($P = 0.038$, $R^2 = 0.216$, $r = -0.465$) (Fig. 5). However, in non-HCC, no correlation was observed between TNR and tumor response according to qEASL % ($P = 0.886$, $R^2 = 0.002$, $r = 0.044$) (Fig. 6).

There was no correlation between TNR and survival in HCC ($P = 0.526$) or non-HCC patients ($P = 0.233$).

DISCUSSION

The main finding of this study is the identification of ETV% as a quantifiable imaging biomarker on preprocedural MRI and CT, which predicts ^{90}Y distribution as measured on immediate postprocedural SPECT. Second, this study validated the relationship between the preferential uptake of ^{90}Y activity to the tumor and tumor response after TARE in patients with HCC.

Recently, TARE was called into question when published results from prospective clinical trials comparing TARE with sorafenib as the standard of care in advanced HCC revealed no difference in survival between both treatments (*16,17*). However, patient selection for TARE in those studies was based mainly on general clinical evaluations rather than individual tumor characteristics. This reflects the currently immature patient selection process in clinical practice, where TARE is oftentimes performed when patients are considered ineligible or not responding to other locoregional therapies such as TACE, which underscores the need for personalized and tumor-specific treatment indications. In this study, the ETV%, reflecting on pathologic tumor viability and vascularity, was identified as a noninvasive imaging biomarker and predictor for ^{90}Y distribution to the tumor after TARE ($P < 0.001$). Thus, the results of this study may help refine patient selection criteria for TARE, consolidating the role of TARE among other intraarterial therapies and improving treatment outcome with minimized toxicity by determining the patients who are most likely to benefit from TARE (*18*).

Previous studies have shown the feasibility and value of quantitative SPECT for the evaluation of the extra- and intrahepatic distribution of ^{90}Y and absorbed dose quantifications after TARE (*19*). More recently, several studies investigating hepatic metastases found CT perfusion imaging and metabolic response assessment using PET predictive of tumor response early after TARE (*20*). This study introduces TNR as a quantitative surrogate on SPECT as a readily applicable predictor for enhancement-based tumor response after TARE in HCC ($P = 0.038$). As morphologic changes of the tumors occur gradually and become measurable on anatomic imaging as late as 2–4 mo after TARE, TNR may thus allow for the evaluation of treatment efficacy immediately after treatment (*21,22*). Such immediate feedback can support timely clinical decision making in rapidly evolving disease processes of liver cancer in a palliative setting.

In addition to ETV% at baseline, the findings of this study suggest that liver cirrhosis represents an additional influencing factor on intrahepatic ^{90}Y distribution. Liver cirrhosis not only is associated with worsened liver function but also causes fundamental structural changes to the parenchyma, with portal hypertension, arterioportal, and hepatovenous shunting being frequently encountered features (*23*). Such conditions may possibly explain why patients with Child–Pugh B demonstrated increased rates of nontarget ^{90}Y delivery ($P = 0.021$) and higher LSF ($P = 0.049$), while, in parallel, demonstrating decreased uptake in tumors, when compared with Child–Pugh A. The reduced dose delivered to the tumor necessarily results in lower response rates while simultaneously increasing the risk of radiation-induced injury to nontumorous parenchyma (*24,25*).

The goal of high and tumor-specific dose delivery provided the rationale for the development of new therapeutic strategies with TARE (*6*). Among others, the concept of radiation segmentectomy was introduced, which represents a possibly curative approach applying high radiation doses to singular tumors restricted to a single or a few segments (*26*). Another approach, called boosted selective internal radiation therapy, targets patients with large HCC with or without portal vein thrombosis for personalized treatment intensification that entails increased amounts of administered ^{90}Y activities (*27*). Patients were selected on the basis of their ^{99m}Tc-MAA scan, quantifications of doses to the tumor and liver, and total injected dose. Boosted selective internal radiation

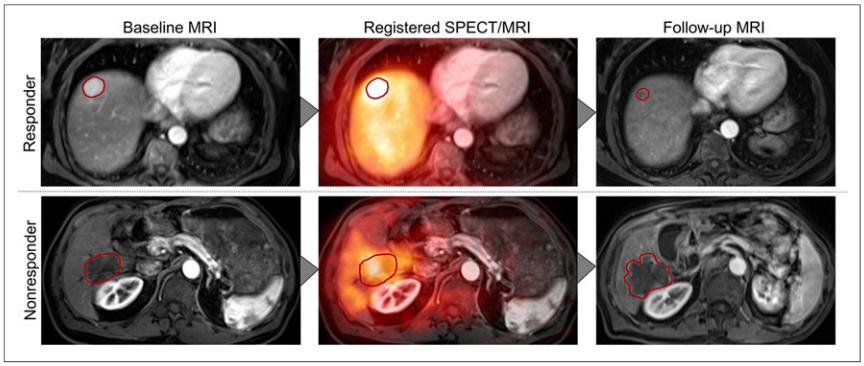

FIGURE 5. Multimodal image analysis. Postprocessing and analyses included volumetric segmentations of dominant tumors on baseline and follow-up MRI, registration of baseline MRI on postprocedural SPECT, and tumor response assessment.

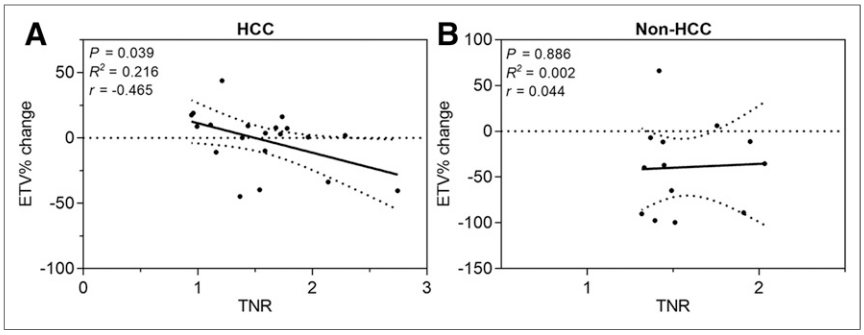

FIGURE 6. Correlation of ^{90}Y distribution and changes of tumor enhancement after TARE. This graph demonstrates that ^{90}Y uptake in dominant tumors correlates with reduction of ETV% according to qEASL tumor response criteria (available for 25 lobar treatments) in HCC (n = 20) (A) but not in non-HCC (n = 13) (B). Intermittent lines indicate 95% confidence interval.

therapy was found to achieve significantly higher tumor doses resulting in improved response rates without compromising patient safety. Although conducted with glass spheres containing higher activity per microsphere, this approach proves the potential and underscores the need for surrogate markers predicting ^{90}Y distribution to achieve better outcomes after TARE.

Hepatic metastases usually show different contrast uptake and washout behavior than HCC (*28,29*). As the vascular density in metastatic tumors such as colorectal cancer metastases is usually lower than for HCC, metastases may lack contrast enhancement on baseline imaging and distinct alterations of contrast uptake dynamics throughout the course of TARE (*22,28*). In the present cohort, a high baseline ETV% was predictive of ^{90}Y distribution to the tumor (P = 0.039), but ^{90}Y distribution did not correlate with tumor response (P = 0.886). Thus, ETV% as an imaging biomarker for tumor-specific ^{90}Y uptake and the dependent tumor response may be applied only for HCC.

This study had several limitations. This is a retrospective study with a relatively small sample size and relatively wide range of imaging intervals. Additionally, tumors of different entities were included in the non-HCC cohort, with potentially varying physiology and enhancement patterns that may affect the ^{90}Y uptake behavior and response to TARE.

Finally, as compared with SPECT, PET may generally provide more advanced quantification techniques and superior spatial resolution (*30*). However, SPECT is currently still more widely available, with higher cost efficiency than PET, which provided the rationale to develop a quantitative SPECT approach in this study (*31*).

CONCLUSION

This study showed the feasibility and prognostic value of ETV% as a quantifiable imaging biomarker on preprocedural MRI and CT, which predicts the relative ^{90}Y distribution on postprocedural SPECT in HCC and non-HCC. However, the relationship between the preferential uptake of ^{90}Y to the tumor and tumor response after TARE could be validated only for HCC. Overall, this study introduces an easily clinically applicable surrogate marker to refine and personalize patient selection for TARE.

DISCLOSURE

Outside the submitted work, Lynn Savic reports grants from a Leopoldina Postdoctoral Fellowship and the Society of Interventional Oncology (SIO); Julius Chapiro reports grants from the German–Israeli Foundation for Scientific Research and Development, Philips Healthcare, Boston Scientific, Guerbet, and SIO; MingDe Lin is a Visage Imaging employee; Lynn Savic, Julius Chapiro, and MingDe Lin report grants from the National Institutes of Health (NIH/NCI R01 CA206180); Isabel Schobert reports grants from the Biomedical Education Program (BMEP). No other potential conflict of interest relevant to this article was reported.

ACKNOWLEDGMENTS

We thank Chi Liu, Brian Letzen, Sophie Antonia Stark, Paula Marie Oestmann, Clinton Wang, Adam Nelson, Neil Whiteside, Matt Gregory, Brian Patchell, Yanhong Deng, and Geliang Gan for their support and technical and statistical advice.

REFERENCES

1. Bray F, Ferlay J, Soerjomataram I, Siegel RL, Torre LA, Jemal A. Global cancer statistics 2018: GLOBOCAN estimates of incidence and mortality worldwide for 36 cancers in 185 countries. *CA Cancer J Clin.* 2018;68:394–424.
2. Lozano R, Naghavi M, Foreman K, et al. Global and regional mortality from 235 causes of death for 20 age groups in 1990 and 2010: a systematic analysis for the global burden of disease study 2010. *Lancet.* 2012;380:2095–2128.
3. Thomas MB, Zhu AX. Hepatocellular carcinoma: the need for progress. *J Clin Oncol.* 2005;23:2892–2899.
4. Haddad AJ, Bani Hani M, Pawlik TM, Cunningham SC. Colorectal liver metastases. *Int J Surg Oncol.* 2011;2011:285840.
5. Talenfeld AD, Sista AK, Madoff DC. Transarterial therapies for primary liver tumors. *Surg Oncol Clin N Am.* 2014;23:323–351.
6. Kallini JR, Gabr A, Salem R, Lewandowski RJ. Transarterial radioembolization with yttrium-90 for the treatment of hepatocellular carcinoma. *Adv Ther.* 2016;33:699–714.
7. Venkatanarasimha N, Gogna A, Tong KTA, et al. Radioembolisation of hepatocellular carcinoma: a primer. *Clin Radiol.* 2017;72:1002–1013.
8. Piana PM, Bar V, Doyle L, et al. Early arterial stasis during resin-based yttrium-90 radioembolization: incidence and preliminary outcomes. *HPB (Oxford).* 2014;16:336–341.
9. Badiyan S, Bhooshan N, Chuong MD, et al. Correlation of radiation dose and activity with clinical outcomes in metastatic colorectal cancer after selective internal radiation therapy using yttrium-90 resin microspheres. *Nucl Med Commun.* 2018;39:915–920.
10. Liu DM, Salem R, Bui JT, et al. Angiographic considerations in patients undergoing liver-directed therapy. *J Vasc Interv Radiol.* 2005;16:911–935.
11. Ito S, Kurosawa H, Kasahara H, et al. ^{90}Y bremsstrahlung emission computed tomography using gamma cameras. *Ann Nucl Med.* 2009;23:257–267.
12. Shady W, Sotirchos VS, Do RK, et al. Surrogate imaging biomarkers of response of colorectal liver metastases after salvage radioembolization using ^{90}Y-loaded resin microspheres. *AJR.* 2016;207:661–670.
13. Chapiro J, Wood LD, Lin M, et al. Radiologic-pathologic analysis of contrast-enhanced and diffusion-weighted MR imaging in patients with HCC after TACE: diagnostic accuracy of 3D quantitative image analysis. *Radiology.* 2014;273:746–758.
14. Chapiro J, Duran R, Lin M, et al. Transarterial chemoembolization in soft-tissue sarcoma metastases to the liver: the use of imaging biomarkers as predictors of patient survival. *Eur J Radiol.* 2015;84:424–430.
15. Mikell JK, Mahvash A, Siman W, Baladandayuthapani V, Mourtada F, Kappadath SC. Selective internal radiation therapy with yttrium-90 glass microspheres: biases and uncertainties in absorbed dose calculations between clinical dosimetry models. *Int J Radiat Oncol Biol Phys.* 2016;96:888–896.
16. Vilgrain V, Abdel-Rehim M, Sibert A, et al; SARAH Trial Group. Radioembolisation with yttrium-90 microspheres versus sorafenib for treatment of advanced

hepatocellular carcinoma (SARAH): study protocol for a randomised controlled trial. *Trials.* 2014;15:474.
17. Chow PHW, Gandhi M. Phase III multi-centre open-label randomized controlled trial of selective internal radiation therapy (SIRT) versus sorafenib in locally advanced hepatocellular carcinoma: the SIRveNIB study [abstract]. *J Clin Oncol.* 2017;35(suppl):4002.
18. Piana PM, Gonsalves CF, Sato T, et al. Toxicities after radioembolization with yttrium-90 SIR-spheres: incidence and contributing risk factors at a single center. *J Vasc Interv Radiol.* 2011;22:1373–1379.
19. Piasecki P, Narloch J, Brzozowski K, et al. The predictive value of SPECT/CT imaging in colorectal liver metastases response after ^{90}Y-radioembolization. *PLoS One.* 2018;13:e0200488.
20. Shady W, Kishore S, Gavane S, et al. Metabolic tumor volume and total lesion glycolysis on FDG-PET/CT can predict overall survival after ^{90}Y radioembolization of colorectal liver metastases: a comparison with SUVmax, SUVpeak, and RECIST 1.0. *Eur J Radiol.* 2016;85:1224–1231.
21. Riaz A, Kulik L, Lewandowski RJ, et al. Radiologic–pathologic correlation of hepatocellular carcinoma treated with internal radiation using yttrium-90 microspheres. *Hepatology.* 2009;49:1185–1193.
22. Joo I, Kim H-C, Kim GM, Paeng JC. Imaging evaluation following ^{90}Y radioembolization of liver tumors: what radiologists should know. *Korean J Radiol.* 2018;19:209–222.
23. Yu JS, Kim KW, Jeong MG, Lee JT, Yoo HS. Nontumorous hepatic arterial-portal venous shunts: MR imaging findings. *Radiology.* 2000;217:750–756.
24. Kao Y-H, Steinberg JD, Tay Y-S, et al. Post-radioembolization yttrium-90 PET/CT: part 2—dose-response and tumor predictive dosimetry for resin microspheres. *EJNMMI Res.* 2013;3:57.
25. Gabrielson A, Miller A, Banovac F, Kim A, He AR, Unger K. Outcomes and predictors of toxicity after selective internal radiation therapy using yttrium-90 resin microspheres for unresectable hepatocellular carcinoma. *Front Oncol.* 2015;5:292.
26. Riaz A, Gates VL, Atassi B, et al. Radiation segmentectomy: a novel approach to increase safety and efficacy of radioembolization. *Int J Radiat Oncol Biol Phys.* 2011;79:163–171.
27. Garin E, Lenoir L, Edeline J, et al. Boosted selective internal radiation therapy with ^{90}Y-loaded glass microspheres (B-SIRT) for hepatocellular carcinoma patients: a new personalized promising concept. *Eur J Nucl Med Mol Imaging.* 2013;40:1057–1068.
28. Sica GT, Ji H, Ros PR. CT and MR imaging of hepatic metastases. *AJR.* 2000;174:691–698.
29. Shah S, Shukla A, Paunipagar B. Radiological features of hepatocellular carcinoma. *J Clin Exp Hepatol.* 2014;4(suppl):S63–S66.
30. Rahmim A, Zaidi H. PET versus SPECT: strengths, limitations and challenges. *Nucl Med Commun.* 2008;29:193–207.
31. Hicks RJ, Hofman MS. Is there still a role for SPECT–CT in oncology in the PET–CT era? *Nat Rev Clin Oncol.* 2012;9:712–720.

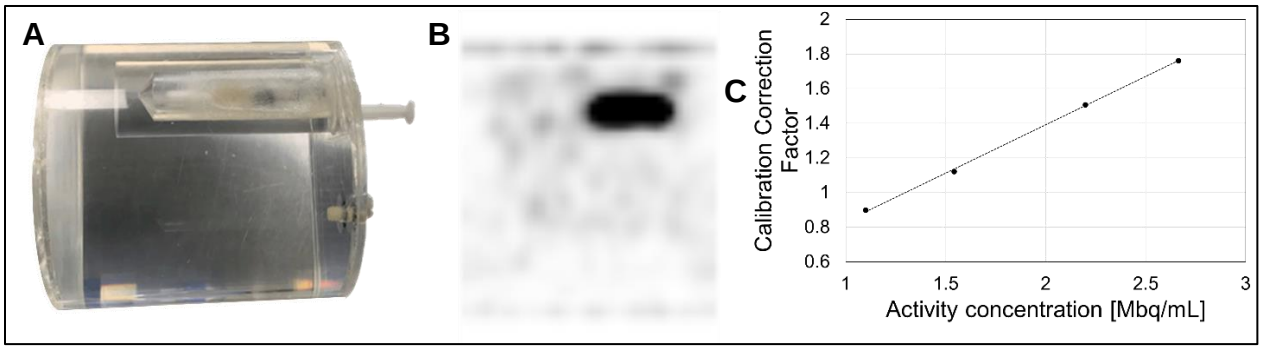

Supplemental Figure 1 Yttrium-90 (^{90}Y) phantom study. A) A cylinder-shaped phantom was filled with saline to mimic the body's water compartment. B) Four 5 mL syringes containing ^{90}Y microspheres of various activity concentrations were scanned sequentially under the same conditions and with the same acquisition protocol as clinical patients. C) Calibration Correction Factors were calculated for each activity concentration in four phantoms.

VII. Curriculum vitae

Mein Lebenslauf wird aus datenschutzrechtlichen Gründen in der elektronischen Version meiner Arbeit nicht veröffentlicht.

VIII. Publication list

Savic LJ, **Schobert IT**, Peters D, Walsh J, Laage-Gaupp F, Hamm CA, Tritz N, Doemel LA, Lin M, Sinusas A, Schlachter T, Duncan JS, Hyder F, Coman D, Chapiro J. Molecular imaging of extracellular tumor pH to reveal and monitor effects of loco-regional therapy on liver cancer microenvironment. Clin Cancer Res. 2020 Jan 15;26(2):428-438. (Impact Factor: 10.199)

Wang CJ, Hamm CA, Savic LJ, Ferrante M, **Schobert I**, Schlachter T, Lin M, Duncan JS, Weinreb JC, Chapiro J, Letzen B. Deep learning for liver tumor diagnosis part II: convolutional neural network interpretation using radiologic imaging features. European radiology. 2019;29(7):3348-57. (Impact Factor: 3.962)

Hamm CA, Wang CJ, Savic LJ, Ferrante M, **Schobert I**, Schlachter T, Lin M, Duncan JS, Weinreb JC, Chapiro J, Letzen B. Deep learning for liver tumor diagnosis part I: development of a convolutional neural network classifier for multi-phasic MRI. European radiology. 2019;29(7):3338-47. (Impact Factor: 3.962)

Schobert I, Chapiro J, Nezami N, Hamm CA, Gebauer B, Lin M, Pollak J, Saperstein L, Schlachter T, Savic LJ. Quantitative Imaging Biomarkers for (90)Y Distribution on Bremsstrahlung SPECT After Resin-Based Radioembolization. J Nucl Med. 2019;60(8):1066-72. (Impact Factor: 7.354)

Review Article
Schobert I, Chapiro J, Pucar D, Saperstein L, Savic LJ. Fluorodeoxyglucose PET for Monitoring Response to Embolotherapy (Transarterial Chemoembolization) in Primary and Metastatic Liver Tumors. PET Clin 2019;14:437-445.

IX. Acknowledgements

Finishing my MD/PhD represents a milestone in my scientific and my personal development. The experiences and knowledge I gained helped me to grow and open up new perspectives and I am very grateful for everyone who contributed and supported me.

First of all, I would like to thank Prof. Dr. Bernhard Gebauer, for the opportunity to pursue my MD/PhD under his supervision and for supporting me and my work at all times. Moreover, I would like to thank Dr. Julius Chapiro for the close mentoring, providing advice, confidence, and for stimulating insightful discussions.

My particular thanks go to Dr. Lynn Jeanette Savic for sharing her scientific expertise, introducing me to various scientific methods, and encouraging the development of my own ideas, always believing in my scientific capabilities. I appreciate a lot, that she listened to my concerns and celebrated my success with me on this journey, going through all highs and lows with patience. While spending many days and hours working together and pushing boundaries for several projects, she taught me a new level of motivation and perseverance. Overall, Dr. Savic was and remains a role model as a scientist and mentor and inspired me to continue research after the completion of my MD/PhD.

I would like to thank the Biomedical Education Program for funding my research exchange. The stipend helped me to focus on my research.

Additionally, I am very thankful for the „Dr. Constantin Cope Medical Student Research Award“, which was awarded by the Society of Interventional Radiology, and is a great honor for my work.

Finally, I would like to thank my parents, Britta and Ulrich, and my siblings, Larissa and Julian, who supported and encouraged me during my studies, my research exchange, and the completion of my MD/PhD.